

## Chapter 2

# Wayfinding and Affine Representations of Urban Environments

While travelling in the city, our primary interest is often in finding the best route from one place to another. Since the wayfinding process is a purposive, directed, and motivated activity (Golledge 1999), the shortest route is not necessarily the best one. If an origin and a destination are not directly connected by a continuous path, wayfinding may include search and exploration actions for which it may be crucial to recognize juxtaposed and distant landmarks, to determine turn angles and directions of movement, and eventually to embed the route in some large reference frame.

In Sect. 1.2.2, we have discussed the neurophysiological evidence confirming that the subjective conceptions of environments in animals are formed in the dMEC cortex, one layer upstream the hippocampus, and then stored in hippocampus, in the animal's spatial memory. The topographical regularity and conditional stability of equilateral tessellating triangles of entorhinal grid cells spanning environmental space suggest that physiological interpretation of space in animals is presumably Euclidean, or at least affine and, thus, can be summarized in terms of points, lines, and surfaces.

It is well-known that the conceptual representations of space in humans do not bear a one-to-one correspondence with actual physical space. For instance, in visual representations given by orthographic projection, for a small view, the components of Euclidean transformations such as translations and rotations about the line of sight do not contribute to an understanding of depth, so that the deformations along the line of sight cannot be visually detected, (Normann et al. 1993).

It has also been demonstrated that human perception of structures from motion (Koenderink et al. 1991 and Luong et al. 1994) has limited capabilities to integrate information across more than two views that would result in the inability to recover true Euclidean metric structures. Since stretches along the line of sight should be invisible, the inability to perceive them was in strong support of the affine nature of human space apprehension.

In vision, affine transformations are usually obtained when a planar object is rotated and translated in space, and then projected into the eye via a parallel projection (Pollick et al. 1997a). Affine concepts have been investigated in the analysis of image motion and the perception of three-dimensional structure from motion, (Beusmans 1993, Pollick 1997b), the recognition of planar forms, away from the

eye, (Wagemans et al. 1994), or in the transformation from visual input to motor output approximating the true Euclidean geometry (Flanders et al. 1992, Pollick et al. 1997a).

In a geometric setting, affine transformations (Zwillinger 1995) are precisely the functions that map straight lines to straight lines, i.e., preserves all linear combination in which the sum of the coefficients is 1. The group of all invertible affine maps of space consists of linear transformations of a point  $\mathbf{x}$  into another point  $\mathbf{y}$  described by some matrix  $\mathcal{A}$  followed by a translation (described by some vector  $\mathbf{a}$ ),

$$\mathbf{y} = \mathcal{A}\mathbf{x} + \mathbf{a}. \quad (2.1)$$

It is known that the affine geometry keeps the concepts of straight lines and parallel lines, but not those of distance between points or value of angles (Busemann et al. 1953). In contrast to (2.1), Euclidean transformations preserve distances between points being a subset of the group of affine transformations such that  $\mathcal{A}$  is a special orthogonal matrix (describing rotations),  $\mathcal{A}\mathcal{A}^\top = 1$ , with the transposed matrix  $\mathcal{A}^\top$ .

Being guided primarily by mental representations of locations and neighborhoods, humans interact with physical environments by travelling through them (Bovy et al. 1990) and by communicating within them with other people by chance, (Hillier et al. 1984).

In this chapter, we address the problem of human understanding of spatial configurations. The process of integrating the local affine models of individual places into the entire cognitive map of the urban area network is very complicated and falls largely within the domain of cognitive science and psychology, but nevertheless the specification of what may be recovered from spatial memory can be considered as a problem of mathematics – “the limits of human perception coincide with mathematically plausible solutions” (Pollick 1997b).

In the forthcoming sections, we use discrete time Markov chains (Markov 1971) to construct the affine representations of urban area networks and demonstrate that our algorithm helps to capture a neighborhood’s inaccessibility, which could expose hidden islands of future deprivation in cities.

## 2.1 From Mental Perspectives to the Affine Representation of Space

Human perception of complex spatial structures is always based on the emergence of simplified models that speed up the interpretation process of environments. They may be supported not only by the structure of Euclidean metric space, but also by weaker and, therefore more general structures of affine and projective spaces, (Faugeras 1995). The occasional overlay of geometrically different structures may give rise to multiple visual illusions.

“Illusions of the senses tell us the truth about perception,” said Jan Evangelista Purkyně (1787–1869), the first Professor of Physiology at the University of Prague

who discovered the Purkinje effect, whereby as light intensity decreases red objects seem to fade faster than blue objects of the same brightness.

Luminance-based repeated asymmetric patterns (RAPs) cause many peoples' visual systems to infer the presence of motion where there is none (Backus et al. 2005). The Japan artist A. Kitaoka has created hundreds of static patterns that appear to move (like that of "rotating snakes" available at <http://www.ritsumei.ac.jp/akitaoka/rotsnake.gif>). The rate of luminance adaptation in human visual cortex is disproportionately faster at high contrast bars coded as deviations from a reference luminance. The tune of the high luminance bars in RAPs by spatial frequency (Backus et al. 2005), the perspective sizes, and the alignment curves (Grzywacz et al. 1991) activates an appropriate set of local velocity detectors in the brain, so that an observer will see the illusory rotation of a disk in "rotating snakes" that can be related by the radius of curvature to motion at constant affine velocity (Pollick 1997b).

The problem with reconstructing of the Euclidean metric properties of space from the affine or projective structures obtained from motion of one or several cameras has always been at the forefront of the interest in computer vision (Koenen et al. 1991, Faugeras 1995). Affine and projective reconstructions of the Euclidean geometry of the real world have been performed from point correspondences by Sparr (1991), as well as from a number of point correspondences in Luong et al. (1994) and Faugeras (1995).

Travelling through the environment provides spatial knowledge of the city for people, and allows common frames of reference to be established (Golledge 1999). It is suggested in wayfinding studies that the spatial models representing the individual places in each neighborhood can be integrated all along the one-dimensional route trajectories into a single layout covering of the entire city.

Supposing the inherent mobility of humans and likeness of their spatial perception aptitudes, one might argue that nearly all people experiencing the city would agree in their judgments on the total number of individual locations in that, in identifying the borders of these locations, and their interconnections. In other words, we assume that spatial experience in humans intervening in the city may be organized in the form of a universally acceptable network.

Well-known and frequently travelled path segments provide linear anchors for certain city districts and neighborhoods that help to organize collections of spatial models for the individual locations into a configuration representing the mental image of the entire city (Lynch 1960). In our study, we assume that the frequently travelled routes are nothing else but the "projective invariants" of the given layout of streets and squares in the city – the function of its geometrical configuration, which remains invariant whatever origin-destination route is considered. The arbitrary linear transformations of the geometrical configuration with respect to which a certain property remains invariant constitute the generalized affine transformations.

It is intuitively clear that if the spatial configuration of the city is represented by a regular graph, where each location represented by a vertex has the same number of neighbors, in absence of other local landmarks, all paths would probably be equally followed by travellers. No linear anchors are possible in such an urban pattern which could stimulate spatial apprehension. However, if the spatial graph of the city is far

from being regular, then a configurational disparity of different places in the city would result in that some of them may be visited by travellers more often than others.

Random walks provide us with an effective tool for the detailed structural analysis of connected undirected graphs exposing their symmetries (Blanchard et al. 2008).

## 2.2 Undirected Graphs and Linear Operators Defined on Them

The human minds cogitations about relations between things, beings, and concepts can often be abstracted as a graph that appears to be the natural mathematical tool for facilitating the analysis (Beck et al. 1969, Biggs et al. 1986).

All elements  $v$  (nodes or vertices) that fall into one and the same set  $V$  are then considered essentially identical, and permutations of them within this set are of no consequence. The symmetric group  $\mathbb{S}_N$  consisting of all permutations of  $N$  elements ( $N$  is the cardinality of the set  $V$ ), forms the symmetry group of  $V$ . If we denote the set of pairwise relationships (edges or links) between all elements of  $V$  by  $E \subseteq V \times V$ , then a graph is a map

$$G(V, E) : E \rightarrow K \subseteq \mathbb{R}_+. \quad (2.2)$$

We emphasize that a graph is an abstract concept, and the definition (2.2) is completely independent of the notions of points and lines which are frequently used to illuminate the structure of the graph. The graph (2.2) is determined by its affinity matrix,  $w_{ij} \geq 0$  if  $i \sim j$ , but  $w_{ij} = 0$  otherwise, and is characterized by the set of its automorphisms<sup>1</sup> describing its symmetries. The definitions and notions of graph theory can be found in Biggs (1974), Bollobas (1979) and Diestrel (2005).

A great deal of effort has been devoted by graph theorists to the study of relations between the structure of the graph  $G$  and the spectra of different matrices associated to it. The relationship between the graph and the eigenvalues and eigenvectors of its adjacency matrix or of the matrix associated to Laplace operators is the main object of spectral graph theory (see Chung 1989a, 1997, deVerdiere 1998, Godsil et al. 2004 and Chap. 3).

### 2.2.1 Automorphisms and Linear Functions of the Adjacency Matrix

It is well-known (see, for example Biggs 1979, Chap. 4) that a transitive permutation group may be represented graphically, and the converse is also true: a graph

---

<sup>1</sup> An automorphism of a graph is a mapping of vertices such that the resulting graph remains isomorphic to the initial one.

gives rise to a permutation group. An automorphism of a graph  $G$  with vertex-set  $V$  and edge-set  $E$  is a permutation  $\Pi$  of  $V$  such that  $(i, j) \in E$  implies that  $(\Pi(i), \Pi(j)) \in E$ . The set of all automorphisms forms a permutation group,  $\text{Aut}(G)$ , acting on  $V$ . For example, the full group of automorphisms of the complete graph  $\mathbb{K}_N$  is the symmetric group  $\mathbb{S}_N$ , since any permutation of the vertices in  $\mathbb{K}_N$  preserves adjacency.

In general,  $\text{Aut}(G)$  includes all admissible permutations  $\Pi \in \mathbb{S}_N$  taking the node  $i \in V$  to some other node  $\Pi(i) \in V$ . The representation of  $\text{Aut}(G)$  consists of all  $N \times N$  matrices  $\Pi_\Pi$ , such that  $(\Pi_\Pi)_{i, \Pi(i)} = 1$ , and  $(\Pi_\Pi)_{i, j} = 0$  if  $j \neq \Pi(i)$ .

A linear transformation of the adjacency matrix

$$Z(\mathbf{A})_{ij} = \sum_{s, l=1}^N \mathcal{F}_{ijsl} A_{sl}, \quad \mathcal{F}_{ijsl} \in \mathbb{R}, \quad (2.3)$$

belongs to  $\text{Aut}(G)$  if

$$\Pi_\Pi^\top Z(\mathbf{A}) \Pi_\Pi = Z\left(\Pi_\Pi^\top \mathbf{A} \Pi_\Pi\right), \quad (2.4)$$

for any  $\Pi \in \text{Aut}(G)$ . It is clear that the relation (2.4) is satisfied if the entries of the tensor  $\mathcal{F}$  in (2.3) meet the following symmetry property:

$$\mathcal{F}_{\Pi(i) \Pi(j) \Pi(s) \Pi(l)} = \mathcal{F}_{ijsl}, \quad (2.5)$$

for any  $\Pi \in \text{Aut}(G)$ . Since the action of the symmetry group preserves the conjugate classes of index partition structures, it follows that any appropriate tensor  $\mathcal{F}$  satisfying (2.5) can be expressed as a linear combination of the following tensors:

$$\left\{ 1, \delta_{ij}, \delta_{is}, \delta_{il}, \delta_{js}, \delta_{jl}, \delta_{sl}, \delta_{ij} \delta_{js}, \delta_{js} \delta_{sl}, \delta_{sl} \delta_{li}, \delta_{li} \delta_{ij}, \delta_{ij} \delta_{sl}, \delta_{is} \delta_{jl}, \delta_{il} \delta_{js}, \delta_{ij} \delta_{il} \delta_{is} \right\}. \quad (2.6)$$

By substituting the above tensors into (2.3) and taking the symmetries, into account we find that any arbitrary linear permutation invariant function  $Z(\mathbf{A})$  defined on a simple undirected graph  $G(V, E)$  must be of the following form,

$$Z(\mathbf{A})_{ij} = a_1 + \delta_{ij} (a_2 + a_3 k_j) + a_4 A_{ij}, \quad (2.7)$$

where  $k_j = \deg(j)$ , and  $a_{1,2,3,4}$  being arbitrary constants.

If we impose, in addition, that the linear function  $Z$  preserves the connectivity,

$$\begin{aligned} \sum_{i \sim j} A_{ij} &= \\ \deg(i) &\equiv k_i \\ &= \sum_{j \in V} Z(\mathbf{A})_{ij}, \end{aligned} \quad (2.8)$$

then it follows that  $a_1 = a_2 = 0$  (since the contributions of  $a_1 N$  and  $a_2$  are indeed incompatible with (2.8)), and the remaining constants should satisfy the relation  $1 - a_3 = a_4$ . By introducing the new parameter  $\beta \equiv a_4 > 0$ , we can reformulate (2.7) in the following form,

$$Z(\mathbf{A})_{ij} = (1 - \beta) \delta_{ij} k_j + \beta A_{ij}. \quad (2.9)$$

It is important to note that (2.8) can be interpreted as a probability conservation relation,

$$1 = \frac{1}{k_i} \sum_{j \in V} Z(\mathbf{A})_{ij}, \quad \forall i \in V, \quad (2.10)$$

and, therefore, the linear function,  $Z(\mathbf{A})$  can be associated to a stochastic process (Blanchard et al. 2008).

By substituting (2.9) into (2.10), we obtain

$$\begin{aligned} 1 &= \sum_{j \in V} (1 - \beta) \delta_{ij} + \beta \frac{A_{ij}}{k_i} \\ &= \sum_{j \in V} T_{ij}^{(\beta)}, \end{aligned} \quad (2.11)$$

in which the operator

$$T_{ij}^{(\beta)} = (1 - \beta) \delta_{ij} + \beta \frac{A_{ij}}{k_i} \quad (2.12)$$

is nothing else but the transition operator of a generalized random walk, for  $\beta \in [0, 1]$ . The operator  $T_{ij}^{(\beta)}$  defines “lazy” random walks for which a random walker stays in the initial vertex with probability  $1 - \beta$ , while it moves to another node randomly chosen among the nearest neighbors with probability  $\beta/k_i$ . In particular, for  $\beta = 1$ , the operator  $T_{ij}^{(\beta)}$  describes the standard random walks extensively studied in the classical surveys of Lovasz (1993) and Aldous et al. 2008 inpreparation

However, if instead of the probability conservation relation (2.10) we require that the linear function  $Z(\mathbf{A})$  is harmonic, i.e.,

$$\sum_{j \in V} Z(\mathbf{A})_{ij} = 0, \quad \forall i \in V, \quad (2.13)$$

then it has been proven by Smola et al. (2003) that (2.9) recovers the generalized Laplace operator

$$L_{ij} = -\frac{a_2}{N} + \delta_{ij} (a_2 + a_3 \deg(i)) - a_3 A_{ij}, \quad (2.14)$$

which describes the diffusion processes characterized by the conservation of mass.

The choice of  $a_2$  and  $a_3$  depends upon the details of the transport process in question. The constant  $a_2$  determines a zero-level transport mode and is usually taken as  $a_2 = 0$ . The Laplace operator (2.14) where  $a_2 = 0$  and  $a_3 = 1$  is called the canonical Laplace operator, (deVerdiere 1998),

$$\mathbf{L}_c = \mathbf{D} - \mathbf{A}, \quad (2.15)$$

where  $\mathbf{D}$  is the diagonal matrix,  $\mathbf{D} = \text{diag}(\deg(1), \dots, \deg(N))$ .

We conclude that the random walk transition operator and the Laplace operator are nothing else but the representations of the set of automorphisms of the graph in the classes of stochastic and harmonic matrices, respectively (Blanchard et al. 2008).

It is also important to mention that the transition probability operator (2.12) describing the set of paths available from  $i \in V$  constitutes the probabilistic analog of the affine transformations remaining invariant the probability distribution  $\pi$ , namely the stationary distribution of random walks.

### 2.2.2 Measures and Dirichlet Forms

The nodes of the graph  $G(V, E)$  can have different weights (or masses) accounted by some measure

$$m = \sum_{i \in V} m_i \delta_i \quad (2.16)$$

specified by any set of positive numbers  $m_i > 0$ . For example, the counting measure assigns to every node a unit mass,

$$m_0 = \sum_{i \in V} \delta_i. \quad (2.17)$$

The Hilbert space  $\mathcal{H}$  (a complete inner product space of functions) on  $\mathbb{R}^V$  is the space of squared summable real-valued functions  $\ell^2(m_0)$  endowed with the usual inner product

$$\langle f | g \rangle = \sum_{i \in V} f(i) g(i),$$

for all  $f, g \in \mathcal{H}(V)$ .

Vectors

$$\mathbf{e}_i = (0, \dots, 1_i, \dots, 0)$$

with a unit at the  $i$ th position representing the node  $i \in V$  form the canonical basis in Hilbert space  $\mathcal{H}(V)$ .

For undirected graphs, the Hilbert space structure on  $\mathbb{R}^E$  is represented by a symmetric Dirichlet form on  $f \in \ell^2(m_0)$  over all edges  $i \sim j$ ,

$$\mathcal{D}(f) = - \sum_{i \sim j} c_{ij} (f(i) - f(j))^2, \quad (2.18)$$

in which  $c_{ij} = c_{ji} \geq 0$ . The quadratic form (2.18) is associated to the elliptic canonical Laplace operator  $\Delta_G$ ,

$$\mathcal{D}(f) = \langle f, \Delta_G f \rangle, \quad f \in \ell^2(m_0), \quad (2.19)$$

which is self-adjoint with respect to the counting measure  $m_0$ .

The canonical Laplace operator can be represented as a product

$$\Delta_G = d^\top d = d d^\top \quad (2.20)$$

of the difference operator  $d : \mathbb{R}^V \rightarrow \mathbb{R}^E$ ,

$$d_{ij}(f) = \begin{cases} f(i) - f(j), & i \sim j, \\ 0, & \text{otherwise,} \end{cases} \quad (2.21)$$

and its adjoint  $d^\top$ .

It is remarkable that the measure  $m_0$  is not the unique measure that can be defined on  $V$ . Given a set of real positive numbers  $m_j > 0$  other measures can be defined by

$$m = \sum_{j \in V} m_j \delta_j. \quad (2.22)$$

The measure associated with random walks defined on undirected graphs,

$$m = \sum_{j \in V} \deg(j) \delta_j, \quad (2.23)$$

is an example.

The transition to the new measure implies a suitable transformation of functions

$$R_m : f_m(j) \rightarrow m_j^{-1/2} f(j), \quad j \in V, \quad (2.24)$$

preserving the notion of elliptic differential operators defined on  $\mathbb{R}^V$ . The Laplace operator self-adjoint with respect to the measure  $m$  is unitary equivalent to  $\Delta_G$ ,

$$L_m = R_m^{-1} \Delta_G R_m, \quad (2.25)$$

where  $R_m$  is the transformation (2.24).

Similarly, the random walks transition operator self-adjoint with respect to the measure  $m$  is unitary equivalent to that of  $T^\beta$ ,

$$T_m = R_m^{-1} T R_m. \quad (2.26)$$

The matrices associated with unitary equivalent operators share many properties: they have the same rank, the same determinant, the same trace, the same eigenvalues (though the eigenvectors will, in general, be different), the same characteristic polynomial and the same minimal polynomial. These can, therefore, serve as isomorphism invariants of graphs. However, two graphs may possess the same set of eigenvalues, but not be isomorphic (deVerdiere 1998).

### 2.3 Random Walks Defined on Undirected Graphs

In the present section, we consider a transition operator determining time reversible random walks of the nearest neighbor type  $(V, \mathbf{T})$  where  $V$  is the vertex set of  $G(V, E)$  and



$$\begin{aligned}
T_{ij} &= \Pr[v_{t+1} = j | v_t = i] > 0 \Leftrightarrow i \sim j, \\
&= \mathbf{D}^{-1} \mathbf{A} \\
&= \deg(i)^{-1}, \text{ iff } i \sim j,
\end{aligned} \tag{2.27}$$

is the one-step probability of a Markov chain  $\{v_t\}_{t \in \mathbb{N}}$  (see Markov) with state space  $V$  (states can repeat). The discrete time random walks introduced on graphs have been studied in Lovasz (1993), Lovasz et al. (1995) and Saloff-Coste (1997).

### 2.3.1 Graphs as Discrete time Dynamical Systems

A finite graph  $G(V, E)$  can be interpreted as a discrete time dynamical system with a finite number of states (Prisner 1995). The temporal evolution of such a dynamical system is described by a “dynamical law” that maps vertices of the graph into other vertices. The Markov transition operator (2.27) is related to the unique Perron-Frobenius operator of the dynamical system, (Mackey 1991).

We can consider a transformation  $\mathcal{S} : V \rightarrow V$  such that it maps any subset of nodes  $U \subset V$  into the set of their neighbors,

$$\mathcal{S}(U) = \{w \in V \mid v \in U, v \sim w\}. \tag{2.28}$$

We denote the result of  $t \geq 1$  successive applications of the transformation to  $U \subset V$  as  $\mathcal{S}_t(U)$ . Then, for every vertex  $v \in V$ , the sequence of successive points  $\mathcal{S}_t(v)$  considered as a function of time is called a trajectory. Given a density function  $f(v) \geq 0$  such that  $\sum_{v \in V} f(v) = 1$ , it follows from (2.27) that the dynamics are given by

$$f^{(t+1)} = f^{(t)} T. \tag{2.29}$$

By definition, the operator  $T^t$  is the Perron-Frobenius operator corresponding to the transformation  $\mathcal{S}$ , since

$$\sum_{v \in U} f(v) T^t = \sum_{\mathcal{S}_t^{-1}(U)} f(v). \tag{2.30}$$

The uniqueness of the Perron-Frobenius operator  $T^t$  is a consequence of the Radon-Nikodym theorem (Shilov et al. 1978).

### 2.3.2 Transition Probabilities and Generating Functions

Given a random walk  $(V, \mathbf{T})$ , we denote the probability of transition from  $i$  to  $j$  in  $t > 0$  steps by

$$p_{ij}^{(t)} = (\mathbf{T}^t)_{ij}. \tag{2.31}$$

The generating function (the Green function) of the transition probability (2.31) is defined by the following power series:

$$\begin{aligned} G_{ij}(z) &= \sum_{t \geq 0} p_{ij}^{(t)} z^t \\ &= (\mathbf{1} - z\mathbf{T})^{-1}, \end{aligned} \quad (2.32)$$

which is convergent inside the unit circle  $|z| < 1$ , the spectral radius of the positive stochastic matrix  $\mathbf{T}$ . Then, it can be readily demonstrated that the limit

$$\mathbf{T}^\infty = \lim_{t \rightarrow \infty} \mathbf{T}^t \quad (2.33)$$

exists as a positive stochastic matrix.

The first hitting probabilities,

$$q_{ij}^{(t)} = \Pr[v_t = j, v_l \neq j, l \neq 1, \dots, t-1 | v_0 = i], \quad q_{ij}^{(0)} = 0, \quad (2.34)$$

are related to the transition probability  $p_{ij}^{(t)}$  by

$$p_{ij}^{(t)} = \sum_{s=0}^t q_{ij}^{(s)} p_{jj}^{(t-s)} \quad (2.35)$$

and can be calculated by means of the generating function

$$F_{ij}(z) = \sum_{t \geq 0} q_{ij}^{(t)} z^t, \quad i, j \in V, \quad z \in \mathbb{C}. \quad (2.36)$$

It follows from (2.34) that the generating functions (2.32) and (2.36) are related (Lovasz et al. 1995) by the equation

$$G_{ij}(z) = F_{ij}(z)G_{jj}(z) \quad (2.37)$$

and, therefore,  $F_{ij}(z)$  is nothing else as the renormalized Green function  $G_{ij}(z)$  in such a way that its diagonal entries become 1.

### 2.3.3 Stationary Distribution of Random Walks

For the operator  $T$  defined on a connected aperiodic graph  $G$ , the Perron–Frobenius theorem see (Graham 1987, Minc 1988, Horn et al. 1990) asserts that its largest eigenvalue  $\mu_1 = 1$  is simple and the eigenvector belonging to it is strictly positive.

A fundamental result on random walks introduced on undirected graphs (Lovasz 1993, Lovasz et al. 1995) is that among all possible distributions

$$\sigma_i = \Pr[v_t = i] \quad (2.38)$$

defined on the graph there exists a *unique* stationary distribution  $\pi : V \rightarrow [0, 1]^N$ , solution of the eigenvalue problem,

$$\pi \mathbf{T} = 1 \pi, \quad (2.39)$$

satisfying the detailed balance equation (Aldous et al. in prepration),

$$\pi_i T_{ij} = \pi_j T_{ji}, \quad (2.40)$$

from which it follows that a random walk considered backwards is also a random walk (time reversibility property). For the nearest neighbor random walk defined by (2.27), the stationary distribution equals

$$\pi_i = \frac{k_i}{2M}, \quad \sum_{i \in V} \pi_i = 1 \quad (2.41)$$

where  $M$  is the total number of edges in the graph, and  $k_i$  is the degree of the node  $i$ .

Given the stationary distribution of random walks, we then define the symmetric transition matrix by

$$\widehat{T}_{ij} = \pi_i^{1/2} T_{ij} \pi^{-1/2} \quad (2.42)$$

and transform it to a diagonal form,

$$\widehat{\mathbf{T}} = \mathbf{U} \Lambda \mathbf{U}^T, \quad (2.43)$$

where  $\mathbf{U}$  is an orthonormal matrix, and  $\Lambda$  is a real diagonal matrix. The symmetric transition matrix for the random walk defined on undirected graphs is simply

$$\widehat{T}_{ij} = \frac{A_{ij}}{\sqrt{k_i k_j}}. \quad (2.44)$$

The diagonal entries of  $\Lambda$ ,

$$1 = \mu_1 > \mu_2 \geq \dots \geq \mu_N \geq -1, \quad (2.45)$$

are the eigenvalues of the transition matrices  $\widehat{\mathbf{T}}$  and  $\mathbf{T}$ . These eigenvalues correspond to the left and right eigenvectors,

$$x_i = \sum_{j \in V} \alpha_j \sqrt{\pi_i} U_{ij}, \quad y_i = \sum_{j \in V} \frac{\alpha'_j}{\sqrt{\pi_i}} U_{ij}, \quad (2.46)$$

( $\alpha_j$  and  $\alpha'_j$  are arbitrary constants) of the transition matrix:

$$\sum_{i \in V} x_i T_{ij} = \mu x_j, \quad \sum_{i \in V} T_{ij} y_i = \mu y_j, \quad \forall j \in V. \quad (2.47)$$

The symmetric matrix  $\widehat{\mathbf{T}}$  as well as its powers can then be written using the spectral theorem,

$$\hat{\mathbf{T}} = \sum_{i=1}^N \mu_i |x_i\rangle \langle y_i|, \quad \hat{\mathbf{T}}^n = \sum_{i=1}^N \mu_i^n |x_i\rangle \langle y_i|. \quad (2.48)$$

It follows from (2.48) that the transition probability  $p_{ij}^{(t)}$  can be computed in the following way,

$$p_{ij}^t = \pi_j + \sum_{l=2}^N \mu_l^t x_{il} y_{jl}. \quad (2.49)$$

### 2.3.4 Continuous Time Markov Jump Process

We can consider a continuous time Markov jump process  $\{w_t\}_{t \in \mathbb{R}_+} = \{v_{\text{Po}(t)}\}$  where  $\text{Po}(t)$  is the Poisson distribution instead of the discrete time Markov chain  $\{v_t\}_{t \in \mathbb{N}}$  (Aldous et al. 2008 in prepration). Supposing that the transition time  $\tau$  is a discrete random variable distributed with respect to the Poisson distribution  $\text{Po}(t)$ , we can write down the corresponding operator with mean 1 exponential holding times as

$$\begin{aligned} p_{ij}^t &= \pi_j + \sum_{l=2}^N x_{il} y_{jl} \sum_{\tau=0}^{\infty} \mu_l^{\tau} \frac{\tau^{\tau} e^{-\tau}}{\tau!} \\ &= \pi_j + \sum_{l=2}^N x_{il} y_{jl} e^{-\lambda_l}, \end{aligned} \quad (2.50)$$

where  $\lambda_l \equiv (1 - \mu_l)$  is the  $l^{\text{th}}$  *spectral gap*. The relaxation processes towards the stationary distribution  $\pi$  of random walks are described by the characteristic decay times  $\tau_l = -1/\ln \lambda_l$ . The asymptotic rate of convergence for (2.50) to the stationary distribution is determined by the spectral gap  $\lambda_2 = 1 - \mu_2$ .

The stationary distribution for general directed graphs is not so easy to describe; it can be very far from a uniform one since the probability that some nodes could be visited may be exponentially small in the number of edges (Lovasz et al. 1995). Moreover, if a directed graph has cycles such that the common divisor of their lengths is larger than 1, the random walk process defined on it does not have any stationary distribution.

## 2.4 Study of City Spatial Graphs by Random Walks

The issues of global connectivity of finite graphs and accessibility of their nodes have always been classical fields of research in graph theory. The level of accessibility of nodes and subgraphs of undirected graphs can be estimated precisely in connection with random walks introduced on them (Volchenkov et al. 2007a, Rosvall et al. 2008). Although random walkers do not interact with each other, the statistical properties of their flows could be highly nontrivial being a detailed fingerprint of the topology. In the present section, we discuss how to analyze and measure the structural dissimilarity between different locations in complex urban networks by means of random walks.

### 2.4.1 Alice and Bob Exploring Cities

We explore the spatial graphs of urban environments following two different strategies of discrete time random walks personified by two walkers, A (Alice) and B (Bob), respectively. Alice and Bob start walking from a location  $x_0 \in V$  randomly chosen among all available locations in the city.

Alice moves at each time step from its actual node  $x_t$  to the next one,  $x_{t+1} \neq x_t$ , selecting it randomly among all other locations adjacent to  $x_t$ , so that Alice's walks constitute a discrete time Markov chain,  $\mathcal{X} = [X_0, X_1, \dots, X_t]$ ,  $t \in \mathbb{N}$ , where

$$\Pr(X_{t+1} = x_{t+1} | X_t = x_t, \dots, X_1 = x_1) = \Pr(X_{t+1} = x_{t+1} | X_t = x_t),$$

for all  $x_0, x_1, \dots, x_{t+1} \in V$ . The Markov chain  $\mathcal{X}$  is determined by its initial site  $x_0$  and the probability transition matrix between the adjacent sites  $x_i \sim x_j$ ,

$$T_{x_i, x_j}^{(A)} = \frac{A_{x_i, x_j}}{\deg(x_i)} \quad (2.51)$$

where  $A_{x_i, x_j}$  is the entry of the  $\{0, 1\}$  adjacency matrix of the city spatial graph, and  $\deg(x_i)$  is the number of neighboring places  $x_i$  is adjacent to. Since the city spatial graph is assumed to be connected and undirected, it is possible to go by  $\mathcal{X}$  with positive probability from any city location to any other one in a finite number of steps, so that the Markov chain  $\mathcal{X}$  is irreducible and time reversible.

The random walk of Bob,  $\mathcal{Y} = [Y_0, Y_1, \dots, Y_t]$ ,  $t \in \mathbb{N}$ , is biased in favor of nodes with the high centrality index,

$$T_{y_i, y_j}^{(B)} = \frac{m_{y_j} A_{y_i, y_j}}{\sum_{y_s \in V} m_{y_s} A_{y_i, y_s}}, \quad (2.52)$$

where  $m_{y_j}$  is the total number of shortest paths between all pairs of distinct locations in the spatial graph of the city that pass through the place  $y_j$ . The random walk  $\mathcal{Y}$  also constitutes a time reversible irreducible Markov chain. However, it is clear that among all places adjacent to his current location Bob always prefers to move into those which occur on the shortest paths in the city graph. In other words, with higher probability, Bob chooses those places that are characterized by the higher betweenness centrality index (i.e., being of a strong choice, in the space syntax terminology) than those that do not. We must stress that the transition operator suggested in (2.52) does not imply that a place that is not a strong choice would never be visited by Bob; however, such a visit is less probable.

Random walks defined by (2.52) are related to various practical studies concerning the city and intercity routing problems, such as the travelling salesman problem, in which the cheapest route is searched (Dantzig et al. 1954). They are also related to pedestrian surveys performed in the framework of space syntax research

that offers evidence that people, in general, prefer to move through the more central (integrated) places in the city (Hillier 2004).

The crucial difference between these two strategies is that while the transition operator (2.51) respects the structure of the graph as captured by its automorphism group being a particular case of the operator (2.12) for  $\beta = 1$ , Bob's shortest path strategy defined by (2.52) does not.

Indeed, the "shortest path strategy" represented above is only one among infinitely many other strategies that walkers – whether they are random or not – would follow while surfing through the city. Given a set of positive masses  $m_i > 0$  characterizing the attraction of a particular place in the city, one can define the correspondent biased walk by (2.52). However, none of them actually fit the set of graph automorphisms, except one of Alice's, with  $m_i = 1$ .

### 2.4.2 *Mixing Rates in Urban Sprawl and Hell's Kitchens*

At the onset of random walks, many new places are visited for the first time and then revisited again until the variations of visiting frequency decreases substantially. Later on, when discovering new nodes takes more time, the rate at which these variations decrease becomes even slower, until the stationary distribution of random walks is eventually achieved.

The rate of convergence,

$$\eta = \lim_{t \rightarrow \infty} \sup \max_{i,j} \left| p_{ij}^{(t)} - \pi_j \right|^{1/t}, \quad (2.53)$$

called the mixing rate (Lovasz et al. 1995) is a measure of how fast the stationary distribution of random walks  $\pi$  can be achieved on the given graph  $G$ . The mixing time,

$$\tau = -\frac{1}{\ln \eta}, \quad (2.54)$$

being a reciprocal quantity for (2.53) measures the expected number of steps required to achieve the stationary distribution of random walks.

If defined for the city spatial graph, the mixing rate (2.53) can be used as a quantitative measure of its structural regularity. If calculated for city spatial graphs, its value is close to 1 if the spatial structure of the urban pattern contains a great deal of repeating elements, but it is below 1 if the city is less ordered. It is known from the space syntax research (see Jiang 1998) that the level of regularity of urban environments is among the key factors that determines people's orientation perception and their wayfinding abilities.

In the Chapter 1, we discussed how similar geometrical elements found in the urban pattern in repetition are converted into a set of twin nodes in the city spatial graph. In particular, an urban pattern developed in an ideal grid is represented by the complete bipartite graph since, for all twin nodes, the rows and columns of

the correspondent adjacency matrix are identical. Twin nodes in the graph have no consequences for random walks.

A spatial structure of suburban sprawl is represented by a star graph, in which individual spaces of the private parking places are connected to a hub associated with the only sinuous central road. Cliental nodes (of degree 1) of a star graph are also twins, being connected to the same hub at the center.

Provided the spatial graph  $G$  contains  $2n$  twin nodes, the correspondent transition probability matrix (2.44) has the  $2n - 2$  multiple eigenvalue  $\mu = 0$ . In particular, the spectrum of a star graph consists of two simple eigenvalues, 1 and  $-1$ , and  $2n - 2$  eigenvalues  $\mu = 0$ . The linear vector subspace which belongs to the multiple eigenvalue  $\mu = 0$  is spanned by  $2n - 2$  orthonormal Faria vectors,

$$\mathbf{f}_s = \frac{1}{\sqrt{2}} [0, \dots, 1, \dots, -1, \dots, 0], \quad s = 1, \dots, 2n - 2,$$

distinguished by the different positions of 1 and  $-1$ . It is clear from (2.49) that, due to  $\mu = 0$ , none of them contributes to the mixing rate (2.53). The transition probability between them is independent of time,  $p_{ij}|_{i,j-\text{twins}} = 1/2(n - 1)$  and can be very small if the spatial representation of the urban pattern contains many twin nodes,  $n \gg 1$ .

In Fig. 2.1, we have represented the comparative diagram for mixing rates of random walks (2.51) defined on the spatial graphs of five compact urban patterns. In order to compare the mixing rates calculated for the organic cities with those found in the urban patterns developed in grids, we have considered a particular neighborhood in Manhattan, in Midtown West, called Hell's Kitchen (also known as

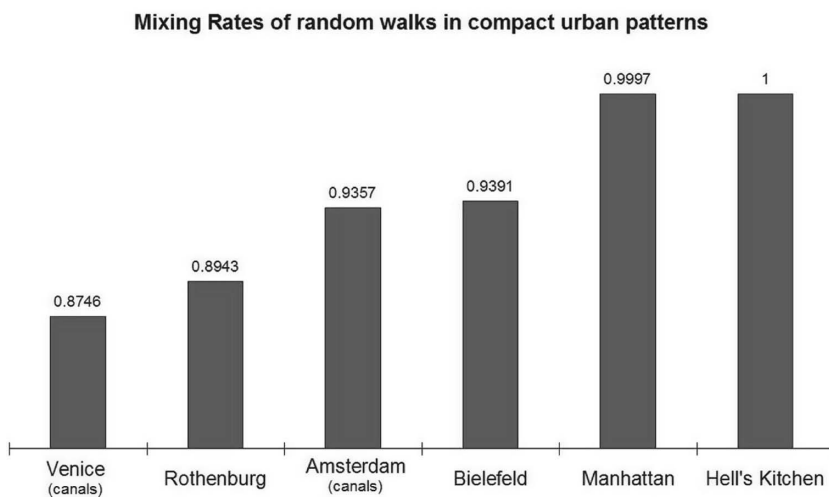


**Fig. 2.1** Mixing rates of random walks on compact urban patterns.

Clinton). This neighborhood includes the area between 34th Street and 57th Street, from 8th Avenue to the Hudson River (the famous selling of the musical “West Side Story,” written by A. Laurents). For us it is essentially interesting since its spatial structure constitutes an ideal grid formed by the standard blocks of  $264 \times 900$  square feet.

The values of the mixing rate allows us to order the compact urban patterns with respect to regularity of their spatial structures – from the city canal network in Venice to the neighborhood in Manhattan. The mixing rate of random walks in Hell’s Kitchen always equals 1!

### 2.4.3 Recurrence Time to a Place in the City

*The wind blows to the south, and goes round to the north; round and round goes the wind,  
and on its circuits the wind returns.*

(Ecclesiastes 1:6)

Beyond any doubt, thanks to connectedness and equi-directedness of the spatial network the edict can work.

The recurrence time of a location indicates how long a random walker must wait to revisit the site. It is known from the work of (Kac 1947) that, for a stationary, discrete-valued stochastic process, the expected recurrence time to return to a state is just the reciprocal of the probability of this state.

The stationary distribution of Alice’s random walk defined by (2.51) is  $\pi_i^{(A)} = k_i/2M$ . Interestingly, it does not depend on the size of the spatial graph  $N$ , but on the total number of edges,  $M$ . Consequently, the recurrence time to a location in the random walk of Alice is inversely proportional to connectivity of the place,

$$r_i^{(A)} = \frac{2M}{k_i} \quad (2.55)$$

and, therefore, depends upon the local property of the place (connectivity).

The stationary distribution of Bob’s random walk defined by (2.52) is the betweenness centrality index of a place (i.e., its global choice) defined by (1.9),  $\pi_i^{(B)} = \text{Choice}(i)$  and, therefore, the recurrence time to a node in Bob’s walk given by

$$r_i^{(B)} = \frac{1}{\text{Choice}(i)} \quad (2.56)$$

can be very different from that in Alice’s walk. The recurrence time (2.56) depends upon the global property of the place in the city.

The key observation related to the stationary distributions of random walks defined on the city spatial graph is that sometimes a highly connected node (a hub) can have a surprisingly low betweenness centrality and vice versa – the local and global properties of nodes are not always positively correlated. In fact, an urban



pattern represented by its spatial graph can be characterized by a certain discrepancy between connectivity and centrality of locations. Such a part-whole relationship between local and global properties of the spaces of motion is known in space syntax theory as intelligibility of urban pattern (Hillier et al. 1984, Hillier 1996). The adequate level of intelligibility is proven to be a key determinant of human behavior in urban environments encouraging people's wayfinding abilities (Jiang et al. 2004).

In order to measure the uncertainty between the connectivity and betweenness centralities of places in the city, we can use the standard Kullback-Leibler distance (the relative entropy between two stationary distributions of random walks,  $\pi^{(A)}$  and  $\pi^{(B)}$ ) (Cover et al. 1991),

$$D\left(\pi^{(B)} \middle| \pi^{(A)}\right) = \sum_{i \in V} \pi_i^{(A)} \log \frac{\pi_i^{(A)}}{\pi_i^{(B)}}. \quad (2.57)$$

The relative entropy (2.57) is always nonnegative and is zero if and only if both probability distributions are equal. However (2.57) does not satisfy the triangle inequality and is not symmetric, so that it is not a true distance.

In Fig. 2.2, we have represented the comparative diagram of the relative entropies between stationary distributions of random walks performed by Alice and Bob in five city spatial graphs. The outstandingly high discrepancy between connectivity and centrality of canals in the city canal network of Venice draws the attention.

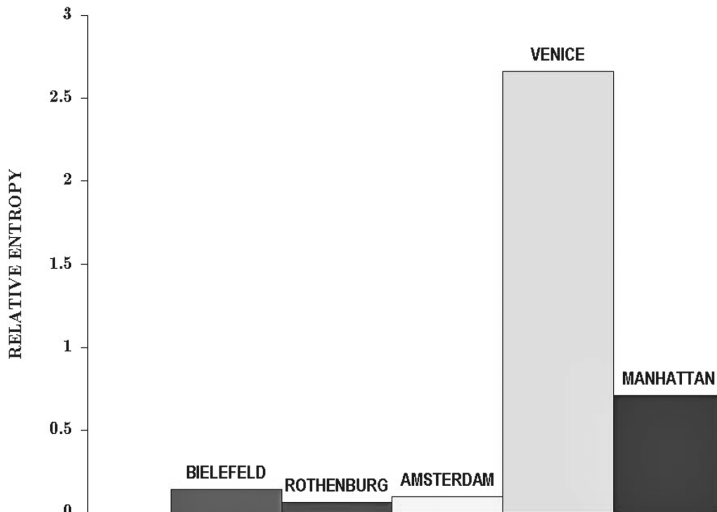


**Fig. 2.2** The relative entropies between stationary distributions of random walks performed by Alice and Bob in five city spatial graphs

### 2.4.4 What does the Physical Dimension of Urban Space Equal?

In classical physics, a traveller has three basic directions in which he or she can move from a particular point – they are physical dimensions of our space.

While simulating the diffusion equation  $u_t = \Delta u$  for the scalar function  $u$  defined on a regular  $d$ -dimensional lattice,  $\mathcal{L}_a = a\mathbb{Z}^d$ , with the lattice scale length  $a$ , one uses its discrete representation,

$$u^{t+1}(x) = \frac{1}{2^d a^2} \left[ \sum_{y \in U_x} u^t(y) - 2^d u^t(x) \right], \quad (2.58)$$

where  $U_x$  is the lattice neighborhood of  $x \in \mathcal{L}_a$ . The cardinal number  $2^d$  is uniform for the given lattice and, therefore, the parameter  $d$  in (2.58) is interpreted as the dimension of Euclidean space.

Being defined on an arbitrary connected graph  $G(V, E)$  the discrete Laplace operator actually has the same form as in (2.58), except when the cardinality number changes to  $2^{\delta_x}$  where

$$\delta_x = \log_2 k_x, \quad k_x = \deg(x) \quad (2.59)$$

it may be considered as the local analog of the physical dimension at the node  $x \in V$  (Volchenkov et al. 2007c).

An interesting question arises concerning (2.59), namely it is possible to define a global dimensional property of the graph that can be considered as the dimension of space? Below, we show that this can be done on a statistical ground, by estimating the spreading of a set of independent random walkers. In information theory (Cover et al. 1991), such a spreading is measured by means of the entropy rate, the informational analog of the physical dimension of space.

Random walks performed by Alice and Bob on undirected spatial graphs are both Markov chains. The number of all possible paths on the graphs grows exponentially with the length of paths  $n$ . Therefore the probability to observe a long enough typical random path  $\{X_1 = x_1, \dots, X_n = x_n\}$  decreases asymptotically exponentially,

$$2^{-n(H(\mathcal{X})+\varepsilon)} \leq \Pr[\{X_1 = x_1, \dots, X_n = x_n\}] \leq 2^{-n(H(\mathcal{X})-\varepsilon)} \quad (2.60)$$

where the parameter  $nH(\mathcal{X})$  measuring the uncertainty of paths in random walks (*entropy*) grows asymptotically linear with  $n$  at a rate  $H(\mathcal{X})$  which is, therefore, called the entropy rate. Since random walks performed by Alice and Bob on the undirected spatial graphs are both irreducible and aperiodic, the corresponding entropy rates are independent of the initial distribution, the probability to chose a certain location in the city as a starting point for a walk. Indeed, the value of  $H(\mathcal{X})$  depends upon the strategy of random walks and, in general,  $H_A \neq H_B$  for any Markov chain  $\mathcal{X}$  (Cover et al. 1991):

$$H_{A,B} = - \sum_{x_i, x_j \in V} \pi^{(A,B)} T_{x_i x_j}^{(A,B)} \log_2 \left( T_{x_i x_j}^{(A,B)} \right). \quad (2.61)$$

As usual, in (2.61) we assume that  $0 \cdot \log(0) = 0$ . In information theory, the entropy rate (2.61) is important as a measure of the average message size required to describe a stationary ergodic process (Cover et al. 1991); provided Alice and Bob use the binary code in their routing reports, they need approximately  $nH_A(\mathcal{X})$  and  $nH_B(\mathcal{X})$  bits, respectively, in order to describe the typical path of length  $n$ . The entropy rates have been used in Boccaletti et al. (2006) and Gomez-Gardenes et al. (2007) as a measure to characterize properties of the topology of complex networks.

Substituting the transition matrix elements and the stationary distribution of Alice's random walks into (2.61), we obtain the entropy rate of an unbiased random walk on a connected undirected network as:

$$H_A = \frac{1}{2M} \sum_{x_i \in V} \delta_x \quad (2.62)$$

where  $\delta_x$  is the local analog of space dimensions defined in (2.59). By the way, the entropy rate of Alice's random walks is just an average of  $\log_2(k_x)$  over all edges in the graph. The entropy rate of Bob's random walks has no simple expression, but can be readily computed numerically – typically, its value exceeds the entropy rate reported by Alice. In Fig. 2.3, we have presented the comparative diagram of entropy rates for both random walks in all five compact urban patterns.

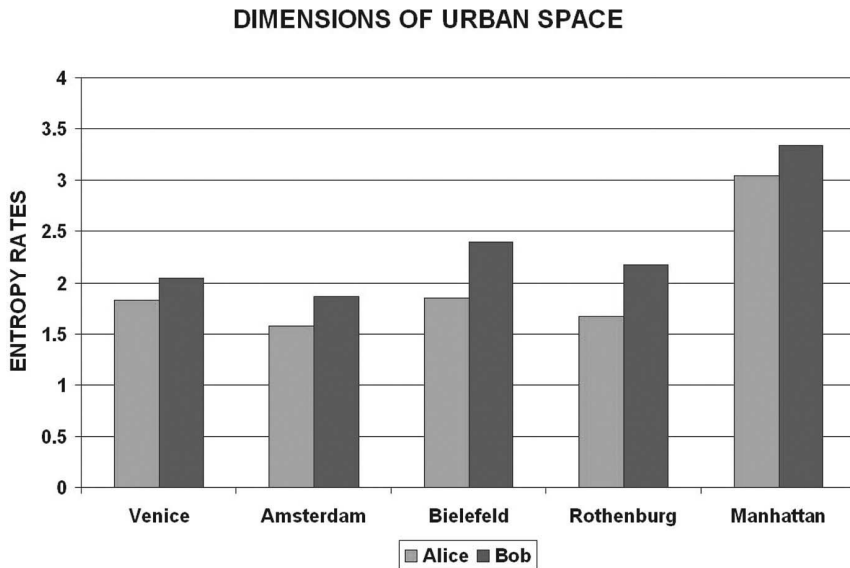


**Fig. 2.3** The entropy rates of random walks reported by Bob and Alice for all five compact urban patterns

Interestingly, the dimensions of random walks defined on spatial graphs of cities which are either organic or had experienced the organic phase in their developments are close to 2, so that their urban space is almost planar. In contrast to them, the relatively regular urban street pattern in Manhattan apparently forms a three-dimensional space.

## 2.5 First-Passage Times: How Random Walks Embed Graphs into Euclidean Space

Discovering important nodes and quantifying differences between them in a graph is not easy since the graph, in general, does not possess the structure of Euclidean space. Representing graph nodes by means of vectors of the canonical basis does not give a meaningful description of the graph since all nodes obviously are equivalent. A natural idea consists of the use of eigenvalues and eigenvectors of a self-adjoint operator defined on the graph in order to define a metric relevant to its topological structure. Spectral methods are popular in applications because they allow a lot of information about graphs to be extracted with minimal computational efforts. The use of self-adjoint operators has become standard in spectral graph theory (Chung 1997), as well as in theory of random walks (Lovasz 1993, Aldous et al. 2008).

### 2.5.1 Probabilistic Projective Geometry

The stationary distribution of random walks  $\pi$  defines a unique measure on the set of nodes  $V$  with respect to which the transition operator ((2.11) for  $\beta = 1$ ) is self-adjoint,

$$\hat{T} = \frac{1}{2} \left( \pi^{1/2} T \pi^{-1/2} + \pi^{-1/2} T^\top \pi^{1/2} \right), \quad (2.63)$$

where  $T^\top$  is the adjoint operator, and  $\pi$  is defined as the diagonal matrix  $\text{diag}(\pi_1, \dots, \pi_N)$ . In particular, for a simple undirected graph, the symmetric operator is defined by (2.44). While interesting in the spectral calculations of random walks characteristics, the symmetric matrix (2.63) is more convenient since its eigenvalues are real and bounded in the interval  $\mu \in [-1, 1]$  and the eigenvectors define an orthonormal basis.

An affine coordinate system on  $V$  is prescribed by an independent set of points for which the displacement vectors  $\mathbf{e}_j = j - i$ ,  $j \in V$ ,  $j \neq i$ , form a basis of  $V$  with respect to the point  $i \in V$ . A displacement vector  $\mathbf{v} = \sum_{j \in V} v_j \mathbf{e}_j$  is identified with the

coordinate  $(N-1)$ -tuple  $(v_1, \dots, \{ \}_i, \dots, v_N)$ , in which the  $i^{\text{th}}$  component is missing. We can associate all points  $V$  with their relative displacement vectors.

The stationary probability distribution  $\pi$  associated with random walks allows us to define a coordinate system in the projective probability space.

Given a symmetric matrix  $w_{ij} \geq 0$  and a vector  $\beta_i \in [0, 1]$ , we can define the transition probability by the kernel (2.27) on  $V$  and its self-adjoint counterpart (2.63). The complete set of real eigenvectors  $\Psi = \{\psi_1, \psi_2, \dots, \psi_N\}$  of the symmetric matrix (2.63),

$$|\psi_i\rangle \hat{T} = \mu_i |\psi_i\rangle,$$

ordered in accordance to their eigenvalues,  $\mu_1 = 1 > \mu_2 \geq \dots \mu_N \geq -1$ , forms an orthonormal basis in  $\mathbb{R}^N$ ,

$$\langle \psi_i | \psi_j \rangle = \delta_{ij}, \quad (2.64)$$

associated to the linear automorphisms of the affinity matrix  $w_{ij}$ , (Blanchard et al. 2008). In (2.64), we have used Dirac's bra-ket notations especially convenient for working with inner products and rank-one operators in Hilbert space.

Given the random walk defined by the operator (2.27), then the squared components of the eigenvectors  $\psi$  have very clear probabilistic interpretations. The first eigenvector  $\psi_1$  belonging to the largest eigenvalue  $\mu_1 = 1$  satisfies  $\psi_{1,i}^2 = \pi_i$  and describes the probability to find a random walker in  $i \in V$ . The norm in the orthogonal complement of  $\psi_1$ ,  $\sum_{s=2}^N \psi_{s,i}^2 = 1 - \pi_i$ , is nothing else, but the probability that a random walker is not in  $i$ .

Looking back it is easy to see that the transition operator (2.63) defines a projective transformation on the set  $V$  such that all vectors in  $\mathbb{R}^N(V)$  collinear to the stationary distribution  $\pi > 0$  are projected onto a common image point.

Geometric objects, such as points, lines, or planes, can be given a representation as elements in projective spaces based on homogeneous coordinates (Möbius 1827). Any vector of the Euclidean space  $\mathbb{R}^N$  can be expanded into  $\mathbf{v} = \sum_{k=1}^N \langle \mathbf{v} | \psi_k \rangle \langle \psi_k |$ , as well as into the basis vectors

$$\psi'_s \equiv \left( 1, \frac{\psi_{s,2}}{\psi_{s,1}}, \dots, \frac{\psi_{s,N}}{\psi_{s,1}} \right), \quad s = 2, \dots, N, \quad (2.65)$$

which span the projective space  $P\mathbb{R}_\pi^{(N-1)}$ ,

$$\mathbf{v} \pi^{-1/2} = \sum_{k=2}^N \langle \mathbf{v} | \psi'_k \rangle \langle \psi'_k |,$$

since we always have  $\psi_{1,x} \equiv \sqrt{\pi_x} > 0$  for any  $x \in V$ . The set of all isolated vertices  $p$  of the graph  $G(V, E)$  for which  $\pi_p = 0$  play the role of the plane at infinity, away from which we can use the basis  $\Psi'$  as an ordinary Cartesian system. The transition to the homogeneous coordinates (2.65) transforms vectors of  $\mathbb{R}^N$  into vectors on the  $(N-1)$ -dimensional hypersurface  $\{\psi_{1,x} = \sqrt{\pi_x}\}$ , the orthogonal complement to the vector of stationary distribution  $\pi$ .

### 2.5.2 Reduction to Euclidean Metric Geometry

The key observation is that in homogeneous coordinates the operator  $\widehat{T}^k \Big|_{P\mathbb{R}_\pi^{(N-1)}}$  defined on the  $(N-1)$ -dimensional hypersurface  $\{\psi_{1,x} = \sqrt{\pi_x}\}$  determines a contractive discrete-time affine dynamical system. The origin is the only fixed point of the map  $\widehat{T}^k \Big|_{P\mathbb{R}_\pi^{(N-1)}}$ ,

$$\lim_{n \rightarrow \infty} \widehat{T}^n \xi = (1, 0, \dots, 0), \quad (2.66)$$

for any  $\xi \in P\mathbb{R}_\pi^{(N-1)}$ , and the solutions are the linear system of points  $\widehat{T}^n \xi$  that hop in the phase space (see Fig. 2.4) along the curves formed by collections of points that map into themselves under the repeated action of  $\widehat{T}$ .

The problem of random walks (2.27, 2.63) defined on finite undirected graphs can be related to a diffusion process which describes the dynamics of a large number of random walkers. The symmetric diffusion process corresponding to the self-adjoint transition operator  $\widehat{T}$  describes the time evolution of the normalized expected number of random walkers,  $\mathbf{n}(t) \pi^{-1/2} \in V \times \mathbb{N}$ ,

$$\dot{\mathbf{n}} = \widehat{L}\mathbf{n}, \quad \widehat{L} \equiv 1 - \widehat{T} \quad (2.67)$$

where  $\widehat{L}$  is the normalized Laplace operator. Eigenvalues of  $\widehat{L}$  are simply related to that of  $\widehat{T}$ ,  $\lambda_k = 1 - \mu_k$ ,  $k = 1, \dots, N$ , and the eigenvectors of both operators are identical. The analysis of spectral properties of the operator (2.67) is widely used in the spectral graph theory (Chung 1997).

It is important to note that the normalized Laplace operator (2.67) defined on  $P\mathbb{R}_\pi^{(N-1)}$  is invertible,

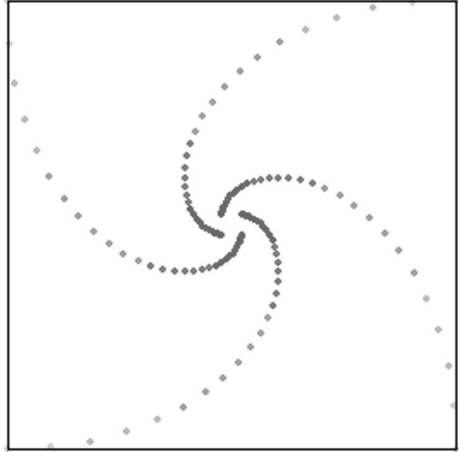


**Fig. 2.4** Any vector  $\xi \in P\mathbb{R}_\pi^{(N-1)}$  asymptotically approaches the origin  $\pi$  under the consecutive actions of the operator  $\widehat{T}$

$$\begin{aligned}\widehat{L}^{-1} &= \left(1 - \widehat{T}\right)^{-1} \\ &= \sum_{n \geq 1} \widehat{T}^n.\end{aligned}\tag{2.68}$$

since  $\widehat{T}^k \Big|_{P\mathbb{R}_\pi^{(N-1)}}$  is a contraction mapping for any  $k \geq 1$ . The unique inverse operator,

$$\widehat{L}^{-1} = \sum_{s=2}^N \frac{|\psi'_s\rangle \langle \psi'_s|}{1 - \mu_s},\tag{2.69}$$

is the Green function (or the Fredholm kernel, the potential of the associated Markov chain) describing long-range interactions between eigenmodes of the diffusion process induced by the graph structure. The convolution with the Green's function gives solutions of inhomogeneous Laplace equations.

In order to obtain a metric on the graph  $G(V, E)$ , one needs to introduce the distances between points (nodes of the graph) and the angles between lines or vectors by determining the inner product between any two vectors  $\xi$  and  $\zeta$  in  $P\mathbb{R}_\pi^{(N-1)}$  as

$$(\xi, \zeta)_T = \left(\xi, \widehat{L}^{-1} \zeta\right).\tag{2.70}$$

The dot product (2.70) is a symmetric real valued scalar function that allows us to define the (squared) norm of a vector  $\xi \in P\mathbb{R}_\pi^{(N-1)}$  with respect to  $(w, \beta)$  by

$$\|\xi\|_T^2 = \left(\xi, \widehat{L}^{-1} \xi\right).\tag{2.71}$$

The (nonobtuse) angle  $\theta \in [0, 180^\circ]$  between two vectors is then given by

$$\theta = \arccos \left( \frac{(\xi, \zeta)_T}{\|\xi\|_T \|\zeta\|_T} \right).\tag{2.72}$$

The Euclidean distance between two vectors in  $P\mathbb{R}_\pi^{(N-1)}$  with respect to  $(w, \beta)$  is defined by

$$\begin{aligned}\|\xi - \zeta\|_T^2 &= \|\xi\|_T^2 + \|\zeta\|_T^2 - 2(\xi, \zeta)_T \\ &= \mathbb{P}_\xi(\xi - \zeta) + \mathbb{P}_\zeta(\xi - \zeta)\end{aligned}\tag{2.73}$$

where  $\mathbb{P}_\xi(\xi - \zeta) \equiv \|\xi\|_T^2 - (\xi, \zeta)_T$  and  $\mathbb{P}_\zeta(\xi - \zeta) \equiv \|\zeta\|_T^2 - (\xi, \zeta)_T$  are the lengths of the projections of  $(\xi - \zeta)$  onto the unit vectors in the directions of  $\xi$  and  $\zeta$ , respectively. It is clear that  $\mathbb{P}_\zeta(\xi - \zeta) = \mathbb{P}_\xi(\xi - \zeta) = 0$  if  $\xi = \zeta$ .

The spectral representations of the Euclidean structure (2.70–2.73) defined for the graph nodes can be easily derived by taking into account that  $\langle i | \psi'_s \rangle = \psi'_{s,i}$ ,  $s = 1, \dots, N$ .

It is obvious from the above formulas that the most important contribution to Euclidean distances defined by (2.73) and (2.71) comes from the second eigenvalue  $\mu_2 < 1$ . The difference  $1 - \mu_2$  is called the spectral gap and defines the bisection of the graph (Cheeger 1969).

### 2.5.3 Expected Numbers of Steps are Euclidean Distances

The structure of Euclidean space introduced in the previous section can be related to a length structure  $V \times V \rightarrow \mathbb{R}_+$  defined on a class of all admissible paths  $P$  between pairs of nodes in  $G$ . It is clear that every path  $P(i, j) \in P$  is characterized by some probability to be followed by a random walker depending on the weights  $w_{ij} > 0$  of all edges necessary to connect  $i$  to  $j$ . Therefore, the path length statistics is a natural candidate for the length structure on  $G$ .

Let us consider the vector  $\mathbf{e}_i = \{0, \dots, 1_i, \dots, 0\}$  that represents the node  $i \in V$  in the canonical basis as a density function. In accordance with (2.71), the vector  $\mathbf{e}_i$  has the squared norm of  $\mathbf{e}_i$  associated to random walks is

$$\|\mathbf{e}_i\|_T^2 = \frac{1}{\pi_i} \sum_{s=2}^N \frac{\psi_{s,i}^2}{1 - \mu_s}. \quad (2.74)$$

It is remarkable that in the theory of random walks (Lovasz 1993) the r.h.s. of (2.74) is known as the spectral representation of the first passage time to the node  $i \in V$ , the expected number of steps required to reach the node  $i \in V$  for the first time starting from a node randomly chosen among all nodes of the graph according to the stationary distribution  $\pi$ . The first passage time,  $\|\mathbf{e}_i\|_T^2$ , can be directly used in order to characterize the level of accessibility of the node  $i$ .

The Euclidean distance between any two nodes of the graph  $G$  calculated in the  $(N - 1)$ -dimensional Euclidean space associated to random walks,

$$K_{i,j} = \|\mathbf{e}_i - \mathbf{e}_j\|_T^2 = \sum_{s=2}^N \frac{1}{1 - \mu_s} \left( \frac{\psi_{s,i}}{\sqrt{\pi_i}} - \frac{\psi_{s,j}}{\sqrt{\pi_j}} \right)^2, \quad (2.75)$$

also gets a clear probabilistic interpretation as the spectral representation of the commute time, the expected number of steps required for a random walker starting at  $i \in V$  to visit  $j \in V$  and then to return back to  $i$  (Lovasz 1993).

The commute time can be represented as a sum,  $K_{i,j} = H_{i,j} + H_{j,i}$ , in which

$$H_{i,j} = \|\mathbf{e}_i\|_T^2 - (\mathbf{e}_i, \mathbf{e}_j)_T \quad (2.76)$$

is the first-hitting time which quantifies the expected number of steps a random walker starting from the node  $i$  needs to reach  $j$  for the first time [Lovasz 1993].

The first hitting time satisfies the equation

$$H_{i,j} = 1 + \sum_{i \sim v} H_{v,j} T_{vi} \quad (2.77)$$

reflecting the fact that the first step takes a random walker to a neighbor  $v \in V$  of the starting node  $i \in V$ , and then it must reach the node  $j$  from there. In principle, the latter equation can be directly used for the computation of the first hitting times; however,  $H_{i,j}$  is not the unique solution of (2.77); the correct definition requires an



appropriate diagonal boundary condition,  $H_{i,i} = 0$ , for all  $i \in V$  (Lovasz 1993). The spectral representation of  $H_{i,j}$  given by

$$H_{i,j} = \sum_{s=2}^N \frac{1}{1-\mu_s} \left( \frac{\psi_{s,i}^2}{\pi_i} - \frac{\psi_{s,i}\psi_{s,j}}{\sqrt{\pi_i\pi_j}} \right), \quad (2.78)$$

seems much easier to calculate. From the obvious inequality  $\lambda_2 \leq \lambda_r$ , it follows that the first-passage times are asymptotically bounded by the spectral gap, namely  $\lambda_2 = 1 - \mu_2$ .

The matrix of first hitting times is not symmetric,  $H_{ij} \neq H_{ji}$ , even for a regular graph. However, a deeper triangle symmetry property (see Fig. 2.5) has been observed by Coppersmith et al. (1993) for random walks defined by the transition operator (2.27). Namely, for every three nodes in the graph, the consequent sums of the first hitting times in the clockwise and the counterclockwise directions are equal,

$$H_{i,j} + H_{j,k} + H_{k,i} = H_{i,k} + H_{k,j} + H_{j,i}. \quad (2.79)$$

We can now use the first hitting times in order to quantify the accessibility of nodes and subgraphs for random walkers.

It is clear from the spectral representations given above that the average of the first hitting times with respect to its first index is nothing else, but the first passage time to the node,

$$\|\mathbf{e}_i\|_T^2 = \sum_{j \in V} \pi_j H_{j,i}. \quad (2.80)$$

The average of the first hitting times with respect to the second index is called the random target access time (Lovasz 1993). It quantifies the expected number of steps required for a random walker to reach a randomly chosen node in the graph (a target). In contrast to (2.80), the random target access time  $\mathfrak{T}_G$  is independent of the starting node  $i \in V$  being a *global* spectral characteristic of the graph,

$$\begin{aligned} \mathfrak{T}_G &= \sum_{j \in V} \pi_j H_{i,j} \\ &= \sum_{k=2}^N \frac{1}{1-\mu_k}. \end{aligned} \quad (2.81)$$

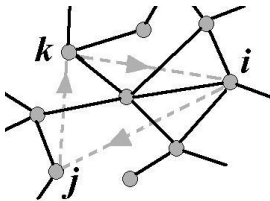


**Fig. 2.5** The triangle symmetry of the first hitting times: the sum of first hitting times calculated for random walks defined by (2.27) visiting any three nodes  $i$ ,  $j$ , and  $k$ , equals the sum of the first hitting times in the reversing direction

The latter equation expresses the so-called random target identity (Lovasz 1993).

Finally, the scalar product  $(\mathbf{e}_i, \mathbf{e}_j)_T$  estimates the expected overlap of random paths toward the destination nodes  $i$  and  $j$  starting from a node randomly chosen in accordance with the stationary distribution of random walks  $\pi$ . The normalized expected overlap of random paths given by the cosine of an angle calculated in the  $(N - 1)$ -dimensional Euclidean space associated to random walks has the structure of Pearson's coefficient of linear correlations that reveals its natural statistical interpretation. If the cosine of the angle (2.72) is close to 1 (zero angles), we conclude that the expected random paths toward both nodes are mostly identical. A value of cosine close to -1 indicates that the walkers share almost the same random paths, but in opposite directions. The correlation coefficient is near 0 if the expected random paths toward the nodes have a very small overlap. As usual, the correlation between nodes does not necessarily imply a direct causal relationship (an immediate connection) between them.

### 2.5.4 Probabilistic Topological Space

In the previous sections we have shown that, given a symmetric affinity function  $w : V \times V \rightarrow \mathbb{R}_+$ , we can always define an Euclidean metric on  $V$  based on the first-access time properties of standard stochastic process, the random walks defined on the set  $V$  with respect to the matrix  $w_{ij} \geq 0$ .

In particular, we can introduce this metric on any undirected graph  $G(V, E)$  converting it in a metric space. The Euclidean distance interpreted as the commute time induces the metric topology on  $G(V, E)$ . Namely, we define the open metric ball of radius  $r$  about any point  $i \in V$  as the set

$$B_r(i) = \left\{ j \in V : K_{i,j}^{1/2} < r \right\}. \quad (2.82)$$

These open balls generate a topology on  $V$ , making it a topological space. A set  $U$  in the metric space is open if and only if for every point  $i \in U$  there exists  $\varepsilon > 0$  such that  $B_\varepsilon(r) \subset U$ , (Burago et al. 2001). Explicitly, a subset of  $V$  is called open if it is a union of (finitely or infinitely many) open balls.

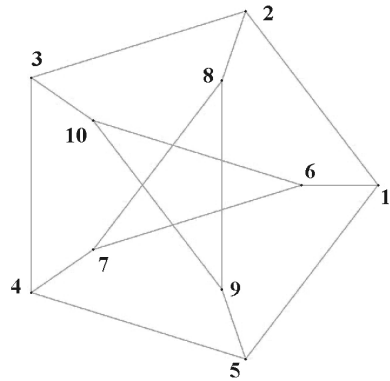
### 2.5.5 Euclidean Embedding of the Petersen Graph

We consider the Euclidean embedding of the Petersen graph (see Fig. 2.6) by random walks as an example.

The Petersen graph is a regular graph,  $k_i = 3$ ,  $i = 1, \dots, 10$ , consisting of 10 nodes and 15 edges,  $\sum_i k_i = 30$ . It constitutes a notorious example for the theory of complex network since the graph nodes cannot be distinguish by its standard methods.

The stationary distribution of random walks on the graph nodes is uniform,  $\pi_i^{(\text{Pet})} = 0.1$ . The spectrum of the random walk transition operator (2.44) defined

**Fig. 2.6** The Petersen graph



on the Petersen graph consists of the Perron eigenvalue,  $\mu_1 = 1$  which is simple, then the eigenvalue  $\mu_2 = 1/3$  with multiplicity 5, and  $\mu_3 = -2/3$  with multiplicity 4. Therefore, in the linear vector space of eigenvectors, there are just three linearly independent eigenvectors, and two eigensubspaces for which the orthonormal basis vectors can be calculated, so that the matrix of basis vectors which we use in (2.74 – 2.75) always has full column dimension.

Random walks embed the Petersen graph into nine-dimensional Euclidean space, in which all nodes have equal norm (2.74),  $\|i\|_T = 3.1464$  meaning that the expected number of steps required to reach a node equals 9.9.

Indeed, the structure of nine-dimensional vector space induced by random walks defined on the Petersen graph cannot be represented visually, however if we choose one node as a point of reference, we can draw its two-dimensional projection by arranging other nodes at distances calculated according to (2.75), and under the angles (2.72) they are with respect to the chosen reference node (see Fig. 2.7).

It is expected that, on average, a random walker starting at node #1 visits any peripheral node (#2, 3, 4, 5) and then returns back in 18 random steps, while 24 random steps are expected for visiting any node in the central component of the graph (#6, 7, 8, 9, 10). Due to the symmetry of the Petersen graph, the diagram displayed

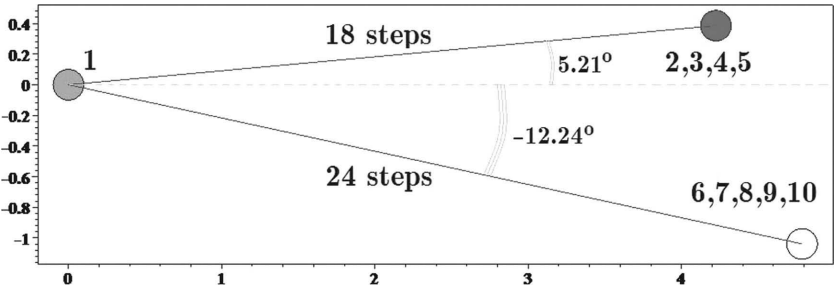


**Fig. 2.7** The two-dimensional projection of the Euclidean space embedding of the Petersen graph drawn with respect to the node #1

in Fig. 2.7 would be essentially the same if we draw it with respect to any other peripheral node (#2,3,4,5). However, it appears to be mirror-reflectd if we draw the figure taking any internal node (#6,7,8,9,10) as the origin. Therefore, we can conclude that the Petersen graph contains two components – the periphery and the core – whose nodes appear to be as much as one-quarter more isolated (18 random steps vs. 24 random steps) than those belonging to the same group.

The positive and negative angles between the nodes belonging to the different components of the Petersen graph indicate that paths of random walkers travelling toward destination nodes essentially, have the same component overlap while they are loosely overlapped and mostly run in opposite directions if they follow the alternative components.

In Fig. 2.8, we have presented the Euclidean space embedding of the Petersen graph by means of the scalar product matrix,  $S_{ij} = (\mathbf{e}_i, \mathbf{e}_j)_T$ . The diagonal elements of  $S_{ij}$  are the first-passage times to the corresponding nodes in the graph, while the entries out of the diagonal give the expected overlaps of random paths toward  $i$  and  $j$ . The eigenvectors belonging to the largest eigenvalues of the matrix  $S_{ij}$  delineate those directions in the vector space along which the scalar product  $(\mathbf{e}_i, \mathbf{e}_j)_T$  has the largest variance. We can represent each node of the Petersen graph by a point in three-dimensional space by regarding the corresponding components of three major eigenvectors as its Cartesian coordinates. It is then clear from Fig. 2.8 that the Petersen graph is bisected in the probabilistic Euclidean space associated with random walks.

In the next section, we apply the method of structural analysis for exploring city spatial graphs.

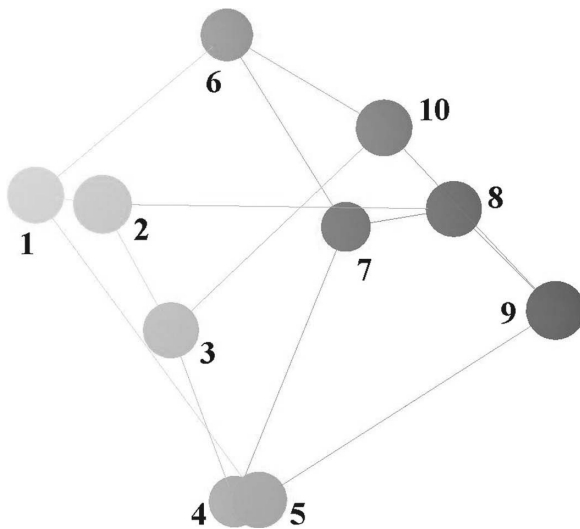


**Fig. 2.8** The 3-D representation of the Petersen graph in the Euclidean space associated with random walks

## 2.6 Case study: Affine Representations of Urban Space

Any connected undirected graph, no matter how complex its structure is, constitutes a normed metric probability space in which the first-passage time to the nodes defines the system of length (Blanchard et al. 2008).

The traffic flow forecasting of first-passage times have been recently studied (Sun et al. 2005) in order to model the wireless terminal movements in a cellular wireless network (Jabbari et al. 1999), in a statistical test for the presence of a random walk component in the repeat sales price index models in house prices [Hill et al. 1999], in the growth modelling of urban agglomerations [Pica et al. 2006], and in many other works where the impact of random walks on city plans and physical landscapes has been considered.

In contrast to all previous studies, in our book, we use discrete time random walks in order to investigate the configuration of urban places represented by means of the spatial graph. In particular, in the present section, we use the first-passage times in order to estimate the levels of accessibility of compact urban patterns. The physical distances between certain locations are of no matter in such a representation and, therefore, random walks are the natural tool for the investigation since, at each time step, a random walker moves to a neighboring place independently of how far it is.

### 2.6.1 *Ghetto of Venice*

The spatial network of Venice that stretches across 122 small islands is comprised of 96 canals which serve as roads.

In March 1516 the Government of the Serenissima Repubblica issued special laws, and the first Ghetto of Europe was instituted in the Cannaregio district, the northernmost part of the city. It was the area where Jews were forced to live and not leave from sunset to dawn. Surrounded by canals, this area was only linked to the rest of the city by two bridges. The quarter had been enlarged later to cover the neighboring Ghetto Vecchio and the Ghetto Nuovissimo. As a result a specific Ghetto canal sub-network arose in Venice weakly connected to the main canals.

The Ghetto existed for more than two and one-half centuries, until Napoleon conquered Venice and finally opened and eliminated every gate (1797). Despite the fact that the political and religious grounds for the ghettoization of these city quarters have disappeared, these components are still relatively isolated from the major city canal network that can be spotted by estimating the first-passage and first hitting times in the network of Venetian canals. Computations of the first hitting times between street and canals in the compact urban patterns have been reported in Volchenkov et al. (2007a).

In Fig. 2.9, we have shown the matrix plot of the first hitting times to the nodes of the spatial graph for 96 canals in the city canal network of Venice.

The variance of the first hitting times to the nodes could help us estimate the quality of spatial representations of urban networks that we use. Already the visual analysis of the variances of the first hitting times to the Venetian canals shows (see

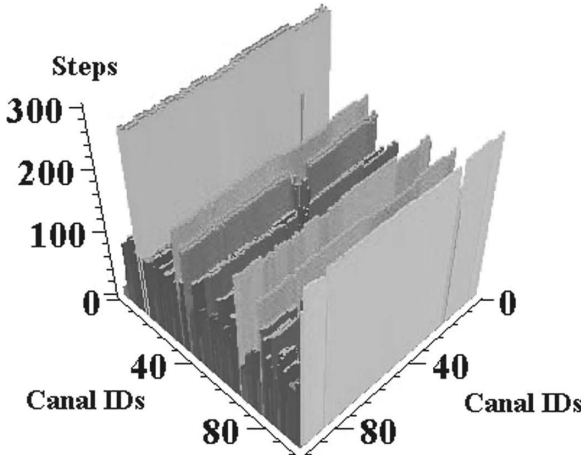


**Fig. 2.9** The matrix plot of the first hitting times between nodes of the spatial graph for 96 canals in the city canal network of Venice

Fig. 2.9) that the values  $H_{i,j}$  vary slightly over the second index  $j$  and, therefore, the averaged first-hitting time (i.e., the first-passage time) to a canal,

$$\|\mathbf{e}_i\|_T^2 = \sum_{j=1}^N \pi_j H_{i,j}, \quad (2.83)$$

can be used as a measure of its accessibility from other canals in the canal network.

The probability distribution of the first-passage times,

$$P(x) = \Pr \left[ i \in G \mid \|\mathbf{e}_i\|_T^2 = x \right], \quad (2.84)$$

allows us to explore the connectedness of the entire canal network in the city. In particular, if the graph contains either groups of relatively isolated nodes, or bottlenecks, they can be visually detected on the probability distribution profile (2.84). This method can facilitate the detection of urban ghettos and sprawl.

The distribution of canals over the range of the first-passage time values is represented by a histogram shown in Fig. 2.10). The height of each bar in the histogram represents the number of canals in the canal network of Venice for which the first-passage times fall into the disjoint intervals (known as bins).

It is fascinating that while most Venetian canals can probably be reached from everywhere in 300 random steps, almost 600 random steps are required in order to reach those canals surrounding the Venetian Ghetto.

It is important to stress the essential difference between the first-passage time to a node as a measure quantifying the global property of the node with respect to other nodes in the graph and the classical integration measure (1.12) related to the simple mean distance  $\ell_i$  from the node  $i$  to any other node in the graph used in the traditional space syntax approach.

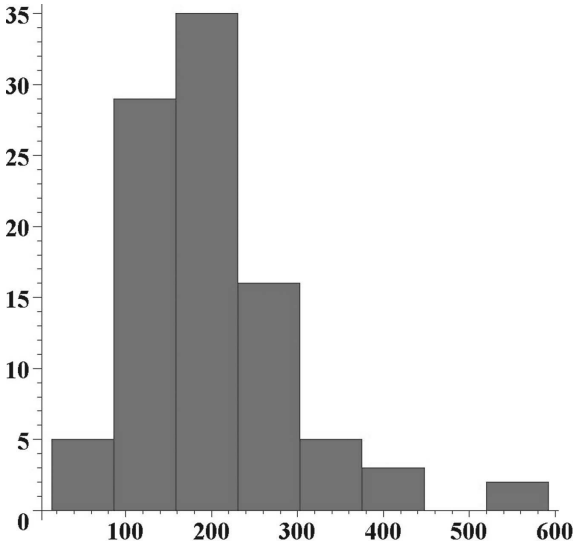


**Fig. 2.10** The histogram of the distribution of canals over the range of the first-passage times in the Venetian canal network

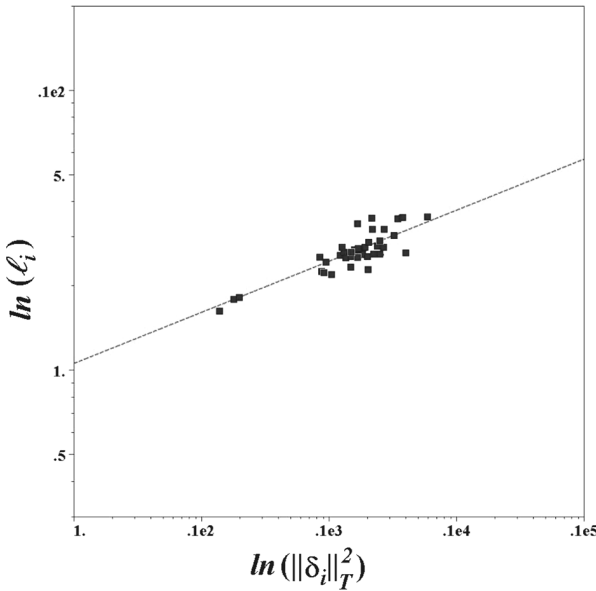


**Fig. 2.11** The scatter plot (in the log-log scale) of the mean distances vs. the value of first-passage times for the network of Venetian canals. The plot indicates a slight, but positive relation between these two characteristics: the slope of regression line equals 0.18. Three data points characterized by the shortest first-passage times and the shortest mean distances represent the main water routes of Venice: the Lagoon, the Giudecca canal, and the Grand canal

The relation between the mean distance (1.8) and the first-passage time to it (2.74) is very complicated and strongly depends on the topology of the graph. In Fig. 2.11, we have shown the scatter plot (in the log-log scale) of the mean distances vs. the value of first-passage times for the network of Venetian canals.

### 2.6.2 Spotting Functional Spaces in the City

Random walks defined on a connected undirected graph partition its nodes into equivalence classes according to their accessibility for random walkers.

The triangle symmetry property (2.79) can be used in order to classify nodes with regard to their accessibility levels (Lovasz 1993). Namely, nodes can be ordered so that  $i \in V$  precedes  $j \in V$  if and only if  $H_{i,j} \leq H_{j,i}$ . Such a relative ordering can be obtained by fixing any  $i \in V$  as a reference node of the graph and then by estimating all other nodes according to the first hitting times difference value,

$$\begin{aligned} \mathfrak{d}_{ij} &= H_{j,i} - H_{i,j} \\ &= \|\mathbf{e}_j\|_T^2 - \|\mathbf{e}_i\|_T^2. \end{aligned} \tag{2.85}$$

Indeed such an ordering is by no means unique, because of the ties. However, if we partition all nodes in the graph by putting  $i \in V$  and  $j \in V$  into the same equivalence class when their reciprocal first hitting times are equal,  $\mathfrak{d}_{ij} \simeq 0$ , (this is an equivalence relation, see Lovasz (1993), then there is a well-defined ordering of equivalence classes, which is obviously independent of any particular reference node  $i \in V$ . Let us mention that, in general, the accessibility equivalence classes do not form connected subgraphs of the initial graph.

The marginal accessibility classes can be of essential practical interest. The nodes in the best accessibility class (characterized by the minimal first hitting time) are easy to reach, but difficult to leave – they act as traps in the graph. The city locations related to public processes of trade, exchange, and government tend to occupy those places which can be easily reached from everywhere. At the same time, in order to increase the chance of plausible contacts between people, it seems reasonable that people could stay in these places longer as if being trapped there. Then, the city locations belonging to the best accessibility class would naturally provide the best places for the public process.

Alternatively, the nodes from the worst accessibility class (the hidden places, characterized by the largest first hitting times) are difficult to reach, but very easy to get out. If found on the city spatial graph, they constitute the optimal location for a residential area where the occasional appearance of strangers is unwilling.

### 2.6.3 Bielefeld and the Invisible Wall of Niederwall

The properties of first hitting times can be used in order to estimate the accessibility of certain streets and districts in the city.



The distribution of first hitting times in the downtown of Bielefeld is of interest since it reveals two structurally different parts (see Fig. 2.12, left) – part “A” keeps its original structure, while part “B” has been subjected to partial redevelopment. Niederwall, the central itinerary crossing the downtown of Bielefeld, constitutes a natural boundary between two parts of the city and conjugates them both.

Computations of first hitting times to the streets in the studied compact urban structures abstracted as spatial graphs in the framework of the street-named approach convinced us that for any given node  $i$  the first hitting times to it,  $H_{ij}$ , fluctuate slightly with respect to the second (destination) index  $j$  in comparison with their typical values and, therefore, the simple partial mean first hitting times,

$$\begin{aligned} h_i(A \rightarrow A) &= N_A^{-1} \sum_{j \in A} H_{ij}, & i \in A, \\ h_i(A \rightarrow B) &= N_B^{-1} \sum_{j \in B} H_{ij}, & i \in A, \\ h_i(B \rightarrow B) &= N_B^{-1} \sum_{j \in B} H_{ij}, & i \in B, \\ h_i(B \rightarrow A) &= N_A^{-1} \sum_{j \in A} H_{ij}, & i \in B, \end{aligned} \quad (2.86)$$

in which  $N_A$  and  $N_B$  are the total number of locations in the A and B parts of the urban pattern in the downtown of Bielefeld consequently, and can be considered good empirical parameters estimating the mutual accessibility of a location within the different parts of the city (Volchenkov et al. 2007a).

Then, the distributions of the simple partial mean first hitting times in the city,

$$\alpha_h(A/B) = \Pr[h_i(A/B \rightarrow A/B) = h], \quad (2.87)$$

can be considered as the empirical estimation of its connectedness.

In Fig. 2.12, we have displayed the distributions of the simple partial mean first hitting times (2.86) to the streets located in the medieval part “A” starting from those located in the same part of Bielefeld downtown, from “A” to “A” (solid line). This has been computed by averaging  $H_{ij}$  over  $i, j \in A$  in (2.86). The dashed line represents the distribution of mean access times to the streets located in the modernized part “B” starting from the medieval part “A” (from “A” to “B”,  $i \in A$  and  $j \in B$ ). One can see that, on average, it takes longer to reach the streets located in “B” starting from “A.” Similar behavior is demonstrated by the random walkers starting from “B” (see Fig. 2.13): on-average, it requires more time to leave a district for another one. Study of random walks defined on the dual graphs helps to detect the quasi-isolated districts of the city.

A sociological survey shows that up to 85,000 people arrive in the city of Bielefeld at the central railway station next to the ancient part “A” during weekends. While exploring the downtown of the city, they eventually reach Niederwall and then usually return to part “A” as if the structural dissimilarity between two parts of the city center clearly visible along Niederwall was an invisible wall. The total number of travellers in part “B” during weekends usually does not exceed 35,000 people, although there are many more old buildings that are potentially attractive to tourists preserved in part “B” than in “A.”

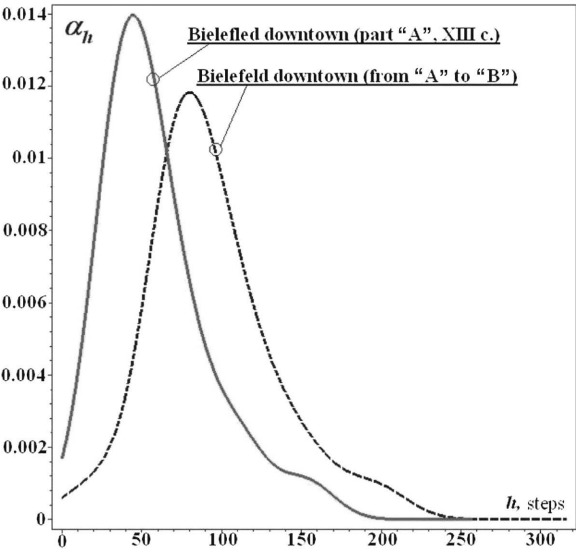


**Fig. 2.12** The distributions, of the simple partial mean first hitting times to the streets located in the medieval part “A” starting from those located in the same part of Bielefeld downtown, from “A” to “A” (solid line). The dashed line presents the distribution of mean access times to the street located in the modernized part “B” starting from the medieval part “A” (from “A” to “B”). On average, it takes longer to reach the streets located in “B” starting from “A”

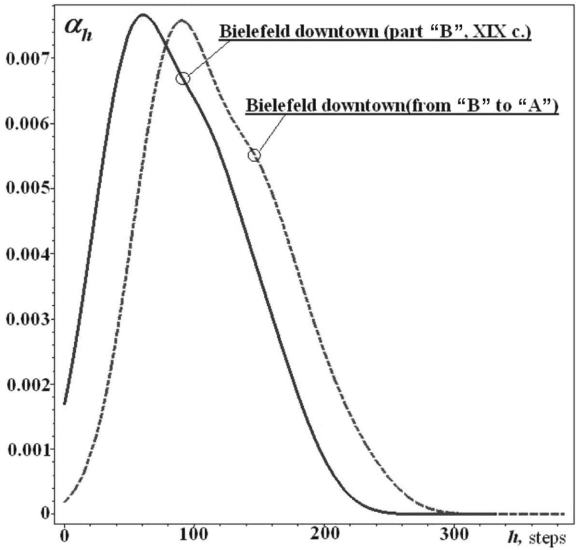


**Fig. 2.13** The distributions of the simple partial mean first hitting times to the streets located in the “B” part starting from “B” (solid line). The dashed line represents the distribution of mean access times to the street located in the “A” part starting from “B”

### 2.6.4 Access to a Target Node and the Random Target Access Time

The notion of isolation acquires the statistical interpretation by means of random walks. The first-passage times in the city vary strongly from location to location. Those places characterized by the shortest first-passage times are easy to reach while many random steps would be required in order to get into a statistically isolated site.

Being a global characteristic of a node in the graph, the first-passage time assigns absolute scores to all nodes based on the probability of paths they provide for random walkers. The first-passage time can, therefore, be considered a natural statistical centrality measure of the vertex within the graph.

The possible relation between the local and global properties of nodes is the most profound feature of a complex network. It is intuitive that the the first-passage time to a node,  $\|\mathbf{e}_i\|_T^2$ , has to be positively related to the time of recurrence  $r_i$ : the faster a random walker hits the node for the first time, the more often he is expected to visit it in the future. This intuition is supported by the expression (2.74) from which it follows that  $\|\mathbf{e}_i\|_T^2 \propto r_i$  provided the sum

$$\sum_{s=2}^N \frac{\psi_{s,i}^2}{(1 - \mu_s)} \simeq \text{Const} \quad (2.88)$$

uniformly for all nodes. The relation (2.88) is by no means a trivial mathematical fact, as we shall see below.

We consider again two different types of random walks personified by Alice and Bob in Sect. 2.4. Let us recall that Alice performs the unbiased random walk defined by the transition operator (2.51) implying no preference between nodes. In contrast to her, while executing his biased random walks defined by (2.52), Bob follows “a strategy” paying attention primarily to those nodes of the highest betweenness centrality.

In Fig. 2.14, we have represented the two-dimensional projection of the probabilistic Euclidean space of 355 locations in Manhattan (New York) set up by the unbiased random walk performed by Alice. Nodes of the spatial graph are shown by disks with radiuses  $\rho \propto k_i$  taken proportional to connectivity of the places. Broadway, a wide avenue in Manhattan which also runs into the Bronx and Westchester County, possesses the highest connectivity and, therefore, is located at the center of the diagram shown in Fig. 2.14. Other places have been located at their Euclidean distances (i.e., the first hitting times) from Broadway calculated accordingly

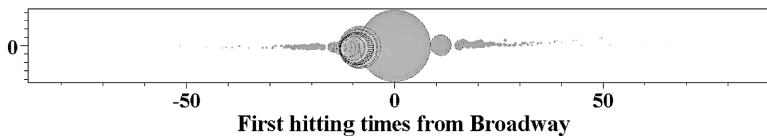


**Fig. 2.14** The two-dimensional projection of the probabilistic Euclidean space of 355 locations in Manhattan (New York) from Broadway set up by the unbiased random walk performed by Alice

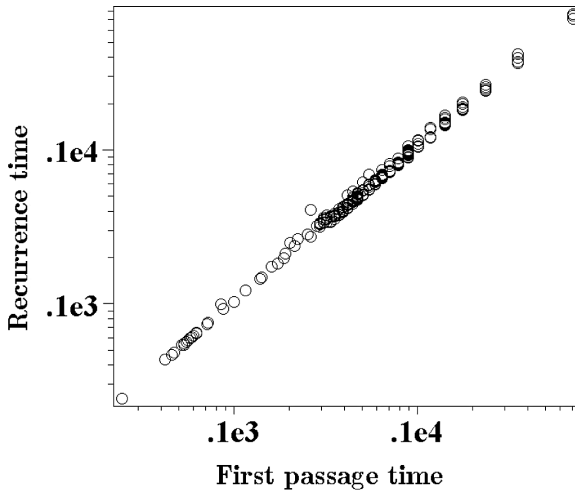


**Fig. 2.15** In the unbiased random walk performed by Alice in Manhattan, the times of recurrence to locations scale linearly with the first-passage times to them

to (2.75), and at the angles calculated by (2.72). It is remarkable that the diagram in Fig. 2.14 displays a nice ordering of places in Manhattan with respect to their connectivity  $k_i$ : the less connected the place, the longer its first hitting time from Broadway.

In the unbiased random walk performed by Alice in Manhattan, the local property of an open space is qualified by its connectivity  $k_i$  which determines the recurrence time of random walks into it (2.55), and the global property of the location is estimated by the first-passage time to it calculated accordingly (2.74). These local and global properties appear to be strongly positively related for every location in the city. In Fig. 2.15, we have presented the log-log plot exhibiting the linear scaling between the first-passage times and recurrence times for the unbiased random walk of Alice.

The relation (2.88) apparently holds for Alice's walks. We can conclude that while the first eigenvector  $\psi_1$  belonging to the largest eigenvalue of the transition operator (2.51) describes the local connectivity of nodes; all other eigenvectors report the global connectedness of the graph.

However, the same correlation is not true for the biased random walks (2.52) performed by Bob.

In Fig. 2.16, we have sketched the central fragment of the two-dimensional projection of Manhattan (New York) set up by the biased random walk of Bob. Radiuses of disks shown in Fig. 2.16 are proportional to the betweenness centrality indices of the correspondent city locations (which are inverse proportional to the recurrence times, in Bob's random walk). The betweenness centrality of Broadway is the highest one, and other places are located at their first hitting times from Broadway calculated according to (2.75) and at the angles calculated by (2.72) for the biased random walks of Bob (2.52). Despite the interesting structural patterns visi-

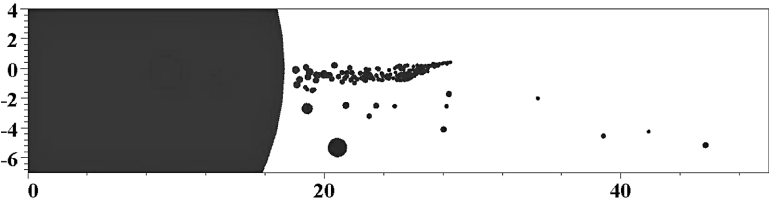


**Fig. 2.16** The central fragment of the two-dimensional projection of the probabilistic Euclidean space of 355 locations in Manhattan (New York) from Broadway set up by the biased random walk performed by Bob

ble in Fig. 2.16, it is, nevertheless, clear that in Bob’s biased random walk there is no direct positive relation between the recurrence times and the first hitting times reported for the different city locations.

The average of the first hitting times  $H_{i,j}$  with respect to its second index expresses the expected number of steps a random walker needs to reach an arbitrary node of the graph (a target) chosen randomly from the stationary distribution of random walks  $\pi$ .

The random target access time can be easily computed accordingly (2.81) provided the spectrum of the random walk transition operator is known. In Fig. 2.17, we have displayed the comparative diagram indicating the values of random target access times for the five compact urban patterns. Beside these bars, we have displayed others with heights equal to the sizes of the studied city spatial graphs. Obviously, the random target access time is an extensive quantity that grows with the size of the city.

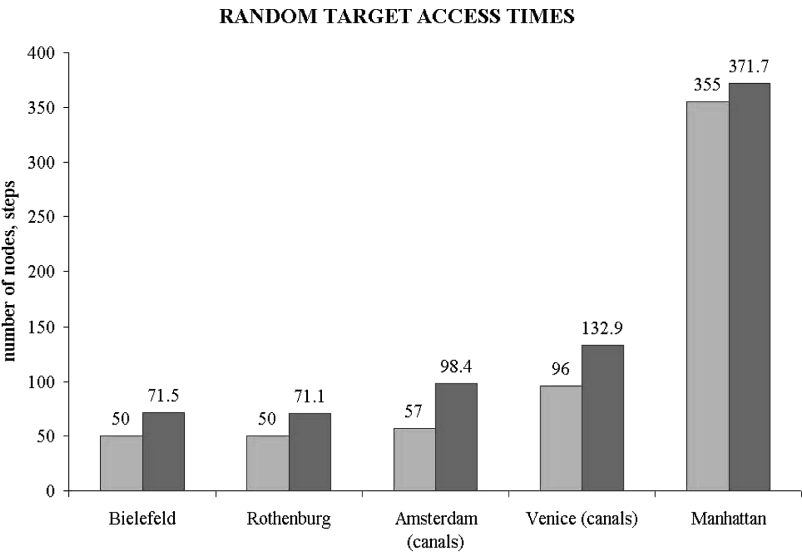


**Fig. 2.17** The comparative diagram of the random target access times for the unbiased random walks and the sizes of spatial graphs for five compact urban patterns. Heights of left bars show the number of nodes in the graphs. Bars on the right indicate the random target access times

### 2.6.5 Pattern of Spatial Isolation in Manhattan

The character and development of Manhattan, the acknowledged heart of New York City, are essentially shaped by geography – Manhattan had only been linked to the other boroughs by bridges and tunnels at the end of the 19th Century. Originally settled around the southern tip dominating New York Harbor, Manhattan expanded northward and encompassed the upper East and West Sides in the mid-19th Century, and the fields above Central Park were settled near the turn of the 19th and 20th Centuries.

The spatial graph representing the structure of the urban pattern in Manhattan constitutes a Euclidean space of dimension 354 over the field of real numbers, endowed with an inner product (2.70). Gram's matrix is a square matrix,

$$\mathcal{G}_{i,j} = (\mathbf{e}_i, \mathbf{e}_j)_T, \quad (2.89)$$

consisting of pairwise scalar products of elements (vectors) representing nodes in this Euclidean space. All Gram matrices are nonnegative definite, and may be positive definite if all vectors in scalar products are linearly independent. The diagonal elements  $\|\mathbf{e}_i\|_T^2$  of the Gram matrix (2.89) define the first-passage times to all places in Manhattan, and the off-diagonal elements,  $(\mathbf{e}_i, \mathbf{e}_j)_T$ ,  $i \neq j$ , are nothing else but the expected overlaps between all pairs of random paths leading to  $i$  and  $j$ .

The Gram matrix (2.89) can be used as a similarity matrix in construction of the three-dimensional visual representations of the spatial graphs of urban area networks. Namely, we can solve the eigenvalue problem,

$$\mathcal{G}\mathbf{u} = \alpha\mathbf{u}, \quad (2.90)$$

and use the components of the first triple of eigenvectors  $\mathbf{u}_1$ ,  $\mathbf{u}_2$ , and  $\mathbf{u}_3$  belonging to the three largest eigenvalues  $\alpha_1 > \alpha_2 > \alpha_3$  of the matrix  $\mathcal{G}$ . These eigenvectors determine the directions in which the spatial graph of the urban area network exhibits the maximal structural similarity. Then, we can use the components of these eigenvectors  $(u_{1,i}, u_{2,i}, u_{3,i})$  to define the coordinates of points representing the spatial locations (nodes) in a visual three-dimensional representation of the spatial graph.

The three-dimensional image of the spatial graph comprising 355 locations in the urban pattern of Manhattan is presented in Fig. 2.18. The radiuses of balls representing the individual places have been taken as proportional to their degrees (the numbers of other locations they are adjacent to in the urban pattern of Manhattan).

The visualization of the affine representation for the urban area network in Manhattan reveals its neighborhood structure, since if random paths originated from a randomly chosen node of the spatial graph and destined towards two different locations are expected to be mostly overlapped, the vertices corresponding to them also appear to be close in the graph representation shown in Fig. 2.18. The groups of places allocated closely in the graph of Fig. 2.18 may represent the geographically localized structural communities with highly probable face-to-face interactions among their dwellers, i.e., neighborhoods.

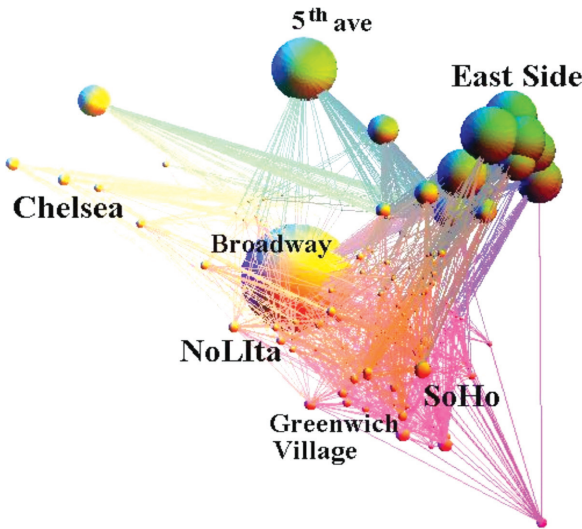


**Fig. 2.18** The three-dimensional representation of the spatial graph of Manhattan based on the first three eigenvectors of the Gram matrix (2.89) belonging to its three maximal eigenvalues. The radiuses of balls representing the individual spatial locations are taken proportional to their degrees

However, the spatial graph of Manhattan (Fig. 2.18) is rather complicated to be analyzed visually. In order to understand its structure, we use the method of kernel density estimations (Wasserman 2005) for the data of first-passage times to all graph nodes. The curve in Fig. 2.19 is the probability density function of the first-passage times (2.84) calculated over the urban pattern of Manhattan.

The first-passage times probability density curve enables us to classify all places in the spatial graph of Manhattan into four groups according to their first-passage

The first group of locations is characterized by the minimal first-passage times; they are probably reached for the first time from any other place of the urban pattern in just 10–100 random navigational steps. These locations are identified as belonging to the downtown Manhattan (at the south and southwest tips of the island) – the Financial District and Midtown Manhattan. These neighborhoods are roughly coterminous with the boundaries of the ancient New Amsterdam settlement founded in the late 17th Century. Both districts comprise the offices and headquarters of many of the city’s major financial institutions such as the New York Stock Exchange and the American Stock Exchange (in the Financial District). Federal Hall National Memorial, which had been anchored by the World Trade Center until the September 11, 2001 terrorist attacks is also encompassed in this area. We might conclude that the group of locations characterized by the best structural accessibility is the heart of the public process in the city (Hillier et al. 1984).

The neighborhoods from the second group comprise the locations that can be reached for the first time in several hundreds to roughly 1,000 random navigational steps from any other place of in urban pattern. In Fig. 2.19, we have marked this zone as a city core. SoHo (to the south of Houston Street), Greenwich Village,

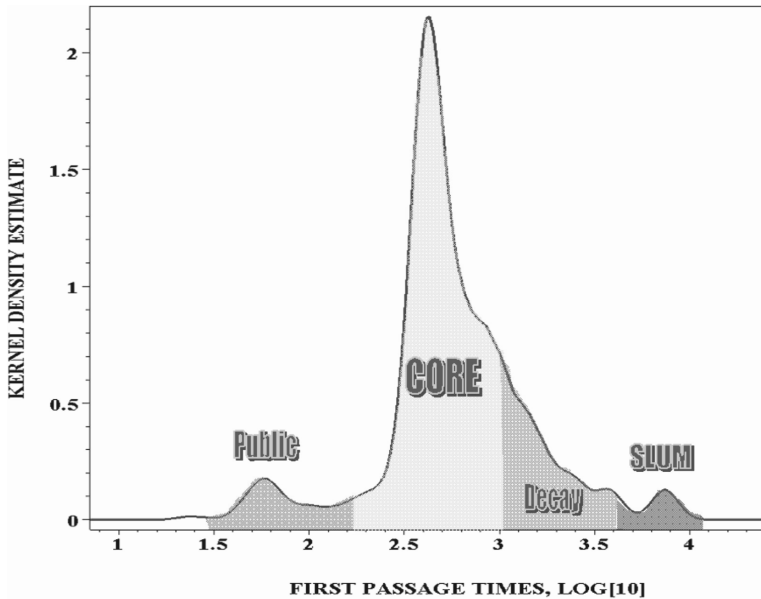


Fig. 2.19 The probability density function of first-passage times in Manhattan.

Chelsea (Hell’s Kitchen), the Lower East Side, and the East Village are among them – they are commercial in nature and known for upscale shopping and the “Bohemian” lifestyle of their dwellers which contributes into New York’s art industry and nightlife.

The relatively isolated neighborhoods, such as the Bowery, some segments in Hamilton Heights and Hudson Heights, Manhattanville (bordered on the south by Morningside Heights), TriBeCa (Triangle Below Canal) and some others can be associated to the third structural category as being reached for the first time from 1,000 to 3,000 random steps starting from a randomly chosen place in the spatial graph of Manhattan. In Fig. 2.19, this category belongs to the decaying tail of the distribution curve.

Interestingly, many locations belonging to the third structural group comprise the diverse and eclectic mix of different social and religious groups. Many famous houses of worship were established there during the late 19th Century – St. Mary’s Protestant Episcopal Church, Church of the Annunciation, St. Joseph’s Roman Catholic Church, and Old Broadway Synagogue in Manhattanville are among them.

The neighborhood of the Bowery in the southern portion of Manhattan had been most often associated with the poor and the homeless. From the early 20th Century, the Bowery became the center of the so-called “b’hoy” subculture of working-class young men frequenting the cruder nightlife. Petty crime and prostitution followed in their wake, and most respectable businesses, the middle-class, and entertainment had fled the area. Today, the dramatic decline has lowered crime rates in the district



to a level not seen since the early 1960s and it continues to fall. Although a zero-tolerance policy targeting petty criminals is being heralded as a major reason for the decrease in crime, no clear explanation for the crime rate's fall has been found.

The last structural category comprises the most isolated segments in the city, mainly allocated in Spanish and East Harlem. They are characterized by the longest first-passage times from 5,000 to more than 7,000 of random steps on the spatial graph in Fig. 2.18. Structural isolation is fostered by the unfavorable confluence of many factors such as the close proximity to Central Park (an area of 340 hectares removed from the otherwise regular street grid), the boundness by the strait of Harlem River separating the Harlem and the Bronx, and the remoteness from the main bridges (the Triborough Bridge, the Willis Avenue Bridge, and the Queensboro Bridge) that connect the boroughs of Manhattan to the urban arrays in Long Island City and Astoria.

Many social problems associated with poverty, from crime to drug addiction, have plagued the area for some time. The haphazard change of the racial composition of the neighborhood occurred at the beginning of the 20th Century together with the lack of adequate urban infrastructure and services fomenting racial violence in deprived communities and made the neighborhood unsafe – Harlem became a slum. The neighborhood had suffered with unemployment, poverty, and crime for quite a long time and even now, despite the sweeping economic prosperity and redevelopment of many sections in the district, the core of Harlem remains poor.

A six-color visual pattern displayed in Fig. 2.20 represents the pattern of structural isolation (quantified by the first-passage times) in Manhattan (darker color corresponds to longer first-passage times). The spatial distribution of isolation in the urban pattern of Manhattan (Fig. 2.20) shows a qualitative agreement with the data on the crime rates in the borough collected in the framework of the Uniform Crime Reporting (UCR) program by the Disaster Center in association with the Rothstein Catalog on Disaster Recovery (USA). Although the UCR data do not include a record of every crime reported to law enforcement, the most accurate number of crimes reported are those involving death, and the least accurate is the number of rapes that are reported. Usually, the high rates of crime are reported from the locations in areas with a large industrial zone or those serving as tourist destinations.

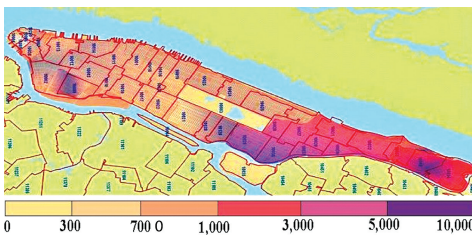


**Fig. 2.20** Isolation map of Manhattan. Isolation is measured by first-passage times to the places. Darker color corresponds to longer first-passage times

According to the latest U.S. Census data (U.S.Census 2006), Manhattan residents have the highest average income (\$73,000) in the United States. Indeed, this average is seriously skewed because of the highest housing costs and other cost of living expenditures that keep pace with the wave of real estate development in a city experiencing tremendous growth. The life and work in many Manhattan neighborhoods, as well as their shapes, are undergoing rapid transformation, although incomes of the majority of New Yorkers are not keeping up with the cost of living.

The mean household income in Manhattan demonstrates a striking spatial pattern which can be analyzed and compared with the pattern of structural isolation quantified by the first-passage times (see Fig. 2.21). We have used the open data reported by the Pratt Center for Community Development (NY) on the mean household income in Manhattan per year for 2003 (indicated by bars in Fig. 2.21) and identified their locations on the isolation map of the city. Although each income bar in general covers a wide range of isolation values, and, therefore, the juxtaposing bars are partially overlapped, the graph in Fig. 2.21 displays a clear tendency positively relating income and the level of accessibility to a neighborhood.

The Justice Mapping Center (JMC) (Brooklyn, NY) uses computer mapping and other graphical depictions of quantitative data to analyze and communicate social policy information. Their approach is based on the plain fact that American society is stratified and that justice, social welfare, and economic development policies are intimately related to particular jurisdictions and neighborhoods, where people of those different social and economic strata live. The analysis of high resettlement neighborhoods in New York City performed by the JMC in October 2006 convincingly shows that the distributions of crime and prison expenditures in Manhattan

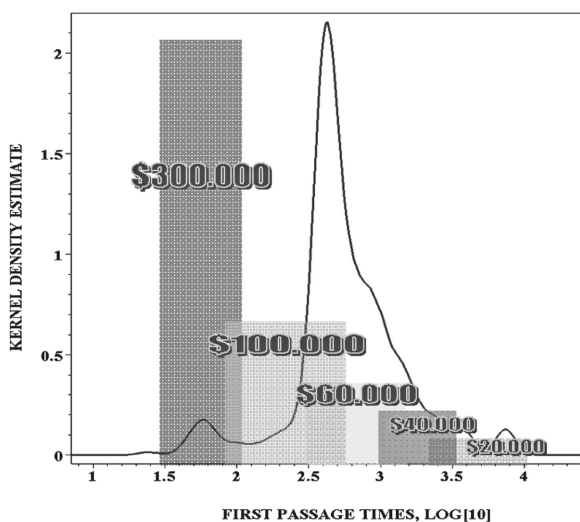


Fig. 2.21 Who makes the most money in Manhattan? (2003)

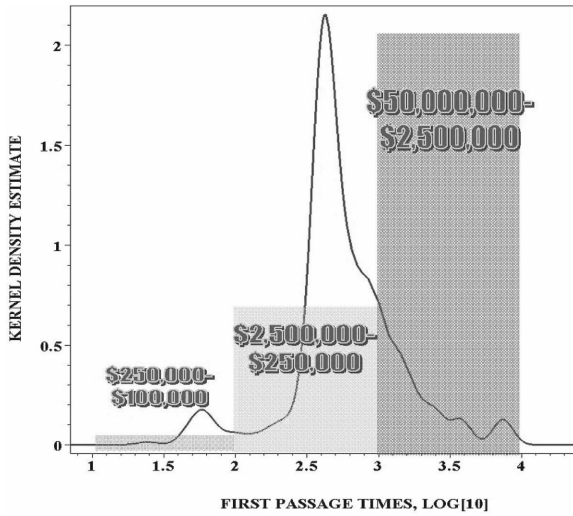


Fig. 2.22 Prison expenditures in Manhattan districts per year (2003)

exhibit a clear spatial pattern. In Fig. 2.22, we have presented the results of comparison between the spatial pattern of prison expenditures in different zip code areas of Manhattan dated to 2003, and the pattern of structural isolations.

The data shown on the diagram Fig. 2.22 positively relates the level of structural isolation of a neighborhood to its prison expenditures.

The relation between the extent of structural isolation and the specified reference levels of prison expenditures can be measured in a logarithmic scale by using decibels (dB). When referring to estimates of isolation by means of first-passage times (FPT), a ratio between two levels inherent to the different locations A and B can be expressed in decibels by evaluating,

$$I_{AB} = 10 \log_{10} \left( \frac{FPT(A)}{FPT(B)} \right), \quad (2.91)$$

where  $FPT(A)$  and  $FPT(B)$  are the first-passage times to A and B, respectively. In Fig. 2.22, all bars representing the amount of prison expenditures in neighborhoods of Manhattan are of the same width corresponding to the increase of isolation by  $I_{AB} = 10$  dB. Similarly, the decibel units can be applied to express the relative growth in prison expenditures (PE) between neighborhoods A and B,

$$PE_{AB} = 10 \log_{10} \left( \frac{PE(A)}{PE(B)} \right), \quad (2.92)$$

The data of Fig. 2.22 represented as a table (see Table 2.1) below demonstrate that prison expenditures show a tendency to increase as isolation worsens.

**Table 2.1** Growth of prison expenditures as isolation worsens

Location category	Increase of isolation (dB)	Prison expenditure growth (dB)
Financial district	10	3.98
City core	10	10
Decay & Slums	10	13.01

**2.6.6 Neubeckum: Mosque and Church in Dialog**

Churches are buildings used as religious places, in the Christian tradition. In addition to being a place of worship, the churches in Western Europe were utilized by the community in other ways, i.e., as a meeting place for guilds. Typically, their location was the focus of a neighborhood, or a settlement.

Today, because of the intensive movement of people between countries, the new national unities out of cultural and religious diversity have appeared. United State’s rich tradition of immigrants has demonstrated the ability of an increasingly multicultural society to unite different religious, ethnic and linguistic groups into the fabric of the country, and many European countries have followed suit. (Portes et al. 2006).

Religious beliefs and institutions have and continue to play a crucial role in new immigrant communities. Religious congregations often provide ethnic, cultural and linguistic reinforcements, and often help newcomers to integrate by offering a connection to social groups that mediate between the individual and the new society, so that immigrants often become even more religious in their new country of residence (Kimon 2001).

It is not surprising that the buildings belonging to religious congregations of newly arrived immigrants are usually located not at the centers of cities in the host country – the changes in function result in a change of location. In Sect. 2.6.5, we have discussed that religious organizations of immigrants in the urban pattern of Manhattan have been usually founded in the relatively isolated locations, apart from the city core, like those in Manhattanville. We have seen that the typical first-passage times to the “religious” places of immigrant communities in Manhattan scale from 1,000 to 3,000 random steps. It is interesting to also check this observation for the religious congregation buildings of recent immigrants in Western Europe.

Despite the mosque and the church being located in close geographic proximity in the city of Neubeckum (see Fig. 2.23), their locations are dramatically different with respect to the entire city structure. The analysis of the spatial graph of the city of Neubeckum by random walks shows that, while the church is situated in a place belonging to the city core, and just 40 random steps are required in order to reach it for the first time from any arbitrary chosen place, a random walker needs 345 random steps to arrive at the mosque. The commute time, the expected number of steps a random walker needs to reach the mosque from the church and then to return, equals 405 steps.



Fig. 2.23 Neubeckum (Westphalia): the church and the mosque in dialog

Spietersstrasse, the street which is parallel to the railway, now is the best accessible place of motion in Neubeckum playing the role of its structural “center of mass;” it can be achieved from any other location in the city in just 20 random steps. If we estimate relative isolation of other places of motion with respect to Spietersstrasse by comparing their first-passage times in the logarithmic scale (2.91), then the location of the church is evaluated by  $I_{\text{Church}} \approx 3 \text{ dB}$  of isolation, and  $I_{\text{Mosque}} \approx 12 \text{ dB}$ , for the mosque.

Indeed, isolation was by no means the aim of the Muslim community. The mosque in Neubeckum has been erected on a vacant place, where land is relatively cheap. However, structural isolation under certain conditions would potentially have dramatic social consequences. Efforts to develop systematic dialogue and increased cooperation based on a reinforced culture of consultations are viewed as essential to deliver a sustainable community.

## 2.7 Summary

We assumed that spatial experience in humans intervening in the city may be organized in the form of a universally acceptable network.

We also assumed that the frequently travelled routes are nothing else but the “projective invariants” of the given layout of streets and squares in the city – the function of its geometrical configuration, which remains invariant whatever origin-destination route is considered.

Based on these two assumptions, we have developed a method that allows us to capture a neighborhood’s inaccessibility.

Any finite graph  $G$  can be interpreted as a discrete time dynamical system with a finite number of states. The temporal evolution of such a dynamical system is described by a “dynamical law” that maps vertices of the graph into other vertices and can be interpreted as the transition operator of random walks. The level of accessibility of nodes and subgraphs of undirected graphs can be estimated precisely in connection with random walks introduced on them, and We have applied this method to the structural analysis of different cities.

Mathematical Analysis of Urban Spatial Networks

Blanchard, P.; Volchenkov, D.

2009, XIV, 184 p. 123 illus., 16 illus. in color., Hardcover

ISBN: 978-3-540-87828-5